Genetic and functional diversification of chemosensory pathway receptors in filarial worms

Sensory receptors of filarial worms

Nicolas J Wheeler[1], Zachary W Heimark[1], Paul M Airs[1], Alexis Mann[1], Lyric C Bartholomay[1], Mostafa Zamanian[1*]

[1] Department of Pathobiological Sciences, University of Wisconsin-Madison, Madison, WI USA
[*] mzamanian@wisc.edu

Abstract

Lymphatic filariasis (LF) afflicts over 60 million people worldwide and leads to severe pathological outcomes in chronic cases. The nematode parasites (Nematoda: Filarioidea) that cause LF require both arthropod (mosquito) intermediate hosts and mammalian definitive hosts for their propagation. The invasion and migration of filarial worms through host tissues are complex and critical to survival, yet little is known about the receptors and signaling pathways that mediate directed migration in these medically important species. In order to better understand the role of chemosensory signaling in filarial worm taxis, we employ comparative genomics, transcriptomics, reverse genetics, and chemical approaches to identify putative chemosensory receptor proteins and perturb chemotaxis phenotypes in filarial worms. We find that chemoreceptor family size is correlated with the presence of environmental (extra-host) stages in nematode life cycles, and that filarial worms contain a compact and highly-diverged chemoreceptor complement and lineage-specific ion channels that are predicted to operate downstream of chemoreceptor activation. In *Brugia malayi,* an etiological agent of LF, chemoreceptor expression patterns correspond to distinct parasite migration events across the life cycle. To interrogate the role of chemosensation in the migration of larval worms, arthropod infectious stage (microfilariae) and mammalian infectious stage (L3) *Brugia* parasites were incubated in nicotinamide, an agonist of the nematode transient receptor potential (TRP) channel OSM-9. Exposure of microfilariae to nicotinamide alters intra-mosquito migration while exposure of L3s reduces chemotaxis towards host-associated cues *in vitro*. Nicotinamide also potently modulates thermosensory responses in L3s, suggesting a polymodal sensory role for *Brugia osm-9*. Reverse genetic studies implicate both *osm-9* and the cyclic nucleotide-gated (CNG) channel subunit *tax-4* in larval chemotaxis towards host serum, and these ion channel subunits do not rescue chemosensory defects in *C. elegans osm-9* and *tax-4* knock-out strains. Together, these data reveal genetic and functional diversification of chemosensory signaling proteins in filarial worms, and encourage a more thorough investigation of clade and parasite-specific facets of nematode sensory receptor biology.

Introduction

Lymphatic filariasis (LF) is a parasitic disease caused by mosquito-borne filarial worms (Nematoda: Filarioidea) belonging to the genera *Wuchereria* and *Brugia*. LF is estimated to affect over 60 million people worldwide, particularly in impoverished tropical regions (1). Infections are associated with chronic disability and physical disfigurement, most commonly resulting from advanced manifestations of lymphedema, hydrocele, and elephantiasis. These gross manifestations yield additional stigmatisation and mental health burdens on those suffering, which in turn can prevent individuals from seeking treatment (2–4). Currently, chemotherapeutic control of LF is mainly achieved through mass drug administration (MDA) of diethylcarbamazine citrate (DEC), ivermectin, albendazole, or combinations of these anthelmintic drugs (5,6). However, the suboptimal efficacy of available drugs against adult parasites, contraindication of DEC in patients with multiple filarial diseases, and the threat of drug resistance underlie efforts to develop new treatment options. A better understanding of the molecular basis of parasite behaviors required for successful transmission and parasitism has the potential to aid LF control efforts.

The filarial worms that cause LF have complex life cycles that require migration through hematophagous arthropod intermediate hosts and vertebrate definitive hosts (7). Microfilariae (mf) released from viviparous females in the human lymphatics must reach the peripheral blood where they can enter the proboscis of feeding mosquito intermediate hosts. In susceptible mosquitoes, larvae burrow out of the mosquito midgut, pass through the hemocoel and invade cells of thoracic flight muscles. Larvae grow and develop over the course of approximately two weeks to the human-infective third larval stage (L3), which migrate to the mosquito head region ready for transmission to the mammalian host (8,9). L3s are deposited onto the skin of vertebrate hosts from the proboscis of feeding mosquitoes and must quickly travel through the bite wound and connective tissues to reach the lymphatic system where they reach sexual maturity (Denham and McGreevy 1977; Bartholomay 2014). While the life cycle of LF parasites are well described, the molecular basis for stage-specific migratory behaviors is unknown.

There is growing evidence that chemosensory and other sensory modalities play an important role in nematode parasite transmission and intra-host migration (11–20). However, most studies have focused on single-host nematode parasites with direct life cycles, which are phylogenetically distant from the vector-borne filarial parasites of clade III. Recent studies using human-infective *Brugia malayi* and feline-infective *Brugia pahangi*, a model species for human LF, reveal the presence of canonical nematode sensory organs (amphids) and robust chemotaxis responses to host-associated cues *in vitro* (21–24). Filarial worms also exhibit genus-specific patterns of intra-host migration (25). These observations strongly suggest an important role for chemosensation and chemotaxis in LF parasitism and provide motivation to dissect the signaling pathways and mediators of sensory behaviors in these medically important parasites.

Chemosensory signaling pathways in the model nematode *Caenorhabditis elegans* are well-characterized (26). G protein-coupled receptors (GPCRs) function as chemoreceptors at the amphid cilia, and activation leads to signaling through cyclic nucleotide-gated channels (CNGs) or transient receptor potential channels (TRPs), depending on cell type (27–30). Each amphid neuron expresses a diverse array of GPCRs, in contrast to the one-receptor-per-cell model in vertebrates (31–33). These pathways have likely evolved to reflect the diversity of nematode life-history traits and environmental cues encountered by different parasite species (12,17–19). Despite superficial conservation of nematode chemosensory

pathways, we hypothesized that there are important differences in chemosensory gene repertoire, patterns of expression, and function among free-living, single-host, and vector-borne parasitic nematodes belonging to diverse clades (Blaxter et al. 1998; Blaxter and Koutsovoulos 2015).

Here, we investigate nematode chemosensory receptor biology in LF parasites and connect *in vitro* and *in vivo* chemotaxis behaviors to chemosensory signaling pathways. We carry out genomic and transcriptomic analyses of putative chemosensory GPCRs (chemoreceptors), CNGs, and TRPs in a pan-phylum context. Using a combination of chemical and reverse genetic approaches, we present the first evidence of *Brugia* chemotaxis behaviors modulated by specific sensory-associated receptors. Lastly, we explore how these data reveal unique aspects of chemosensory biology in these medically important parasites.

Results

Filarial worms contain a compact and unique repertoire of chemoreceptors

To elucidate the putative chemosensory pathway of mosquito-borne filarial worms and to identify and annotate chemoreceptors, we first performed a pan-phylum analysis of 39 nematode genomes (34,35), representing all published filarial genomes and high-quality assemblies across four primary nematode clades (36) (S1 Table, S1 Figure). 10,440 chemoreceptor genes were identified and confidently classified within superfamilies (Str, Sra, Srg) or "solo" families (srz, sro, srsx, srbc, srxa, sra) (S1 File) (37). While the majority of receptors were also annotated at the family level, some clade IIIa/b and clade IV chemoreceptors did not clearly group with the families that were originally described in *C. elegans* (Figure 1A-B, S1 Data). However, each of the 30-100 chemoreceptors found in filarial worm species (clade IIIc) were readily classified into the established 23 nematode chemoreceptor families (37,38). Within these families we found no one-to-one orthologs between filarial parasites and species belonging to other clades, demonstrating the divergence of the filarial chemoreceptor subset. Instead, there have been clear paralogous gene radiations that have resulted in enrichment of the *srx, srab, srbc,* and *srsx* families (Figure 1A-B). Filarial parasites also contain relatively numerous *srw* receptors, but these likely include neuropeptide receptors in addition to some chemoreceptors of environmental peptides (38,39).

Filarial worm genomes contain a reduced subset of chemoreceptors when compared to other parasitic and free-living nematodes, including *C. elegans* and *C. briggsae*, both of which contain over 1200 chemoreceptors (clade V) (Figure 1B) (33,37,38). While it is known that parasitic nematodes contain fewer chemoreceptor genes than *C. elegans*(40,41), and indeed often fewer genes in total(42), our pan-phylum analysis revealed a significant correlation between chemoreceptor gene count and the presence and nature of free-living or environmental stages of each nematode species life cycle (Figure 1C). Parasites that are more host-contained and lack motile environmental stages exhibit more compact chemoreceptor repertoires than those that are exclusively free-living or contain free-living stages (Spearman's rank-order correlation, ρ = -0.813, p = 3.24 x 10^{-10}).

Chromosomal synteny between *Brugia malayi* and *C. elegans* further illustrates the divergence of chemoreceptors in the Filarioidea (Figure 2A). The majority of *C. elegans* chemoreceptors are found on chromosome V (67%) and likely underwent several birth-death cycles that reflect the adaptive needs of encountering new locales (37). Putative *B. malayi* chemoreceptors are primarily found on two

chromosomes, II (31%) and IV (35%), and are clustered by family, suggesting lineage-specific gene duplications.

Brugia malayi *chemoreceptors are associated with sensory tissues and display stage-specific expression patterns*

These comparative data indicate that arthropod-borne filarial worms rely on a small complement of clade and species-specific chemoreceptors to interact with and navigate their host environments. Nematode chemosensation is primarily mediated by anterior amphid sensory structures, and many nematodes also possess caudal chemosensory phasmids associated with male sex organs that likely aid in copulation. In *C. elegans* hermaphrodites and *Strongyloides stercoralis*, a soil-transmitted helminth, chemoreceptors and sensory pathway effectors have been primarily localized to these anterior and posterior structures but can also be found in other non-neuronal cells (11,33). We examined the expression of chemoreceptors in structures implicated in adult filarial worm chemosensation (21,43,44) using RNA-seq of anterior and posterior tissues. *B. malayi* female head, male head, and male tail tissue regions were excised for RNA-seq detection of anterior, posterior, and sex-specific chemoreceptor transcripts. Most chemoreceptor transcripts are preferentially detected in one of these disparate anatomical regions, while a small number show a broader distribution of expression across these regions (Figure 2B, S2 Figure).

We further hypothesized that the unique cues encountered by filarial parasites across developmental time points would be reflected by stage-specific chemoreceptor expression patterns. In *C. elegans*, chemosensory processes coordinate movement towards food or mates and away from pathogens, predators, or noxious substances (45–48). In contrast to the open and less predictable environments navigated by free-living nematodes, filarial worms encounter distinct environmental niches that have strictly patterned transitions. We used staged transcriptomes to analyze the expression of chemoreceptors across the life cycle of *B. malayi* (49) and identified receptors that correspond to migratory landmarks throughout the parasite life cycle (Figure 2A). Expression data show that microfilariae circulating in the bloodstream at 60 days post-infection (DPI) express a larger number of chemoreceptors compared to non-migratory L1 and L2 larvae that are contained within mosquito muscle cells; for instance, only 4 chemoreceptors during the mf/L1 stage in the mosquito have detectable expression (Figure 2A). There is an increase in chemoreceptor representation and expression during the migratory and mammalian-infective L3 stage, as well as in later mammalian stages that undergo migration and potentially engage in mate-seeking behaviors. Together, these analyses show that *B. malayi* expresses distinct sets of chemoreceptors in a sex, tissue, and stage-specific manner.

Filarial worms have a divergent subset of downstream chemosensory pathway receptors

In *C. elegans*, ligand binding of chemoreceptors activates heterotrimeric G proteins that ultimately produce neuronal depolarization via the opening of cyclic nucleotide-gated channels (CNGs) or transient receptor potential channels (TRPs), depending upon cell type (26,33). The CNGs TAX-4 and TAX-2 mediate signaling in amphid neurons ASE, AWC, AWB, ASI, ASG, ASJ, ASK, while the TRPV (vanilloid-type) channels OSM-9 and OCR-2 are necessary for signaling in AWA, ASH, ADF, and ADL (26). To assess the conservation of these downstream signaling pathways in filarial parasites, we mined TRP and CNG channels across nematode genomes to examine interspecies variation in ion channel complements.

We found that filarial worms contain one-to-one homologs of *osm-9*, but do not have homologs of *ocr-3, ocr-4, trpa-1, pkd-2, trp-1,* or *gtl-1* (Figure 3A/C/E, S2 Data). Filarial parasites contain two ocr-1/2-like genes (Bm5691 and Bm14098), but these are more closely related to each other than they are to *C. elegans ocr-1* or *ocr-2* (Figure 3E). In *C. elegans*, OSM-9 and OCR-2 are mutually dependent upon each other for intracellular trafficking to sensory cilia (30). However, cell-specific TRP channel expression patterns and TRP subunit interactions are unknown in filarial parasitic species, and it is not clear which filarial parasite subunit might provide a homologous OCR-2 ciliary targeting function, or indeed if such a trafficking function is necessary. We found homologs of *ocr-3, ocr-4, pkd-2,* and *trp-1* in other clade III species, and the most parsimonious explanation of their absence in filarial worms is that these genes were lost sometime after the divergence of Spirurida and Ascarida (50). Conversely, *trpa-1*, which functions in *C. elegans* mechanosensation in QLQ (51), and *gtl-1*, which functions in ion homeostasis in the *C. elegans* intestine (52), appear to be specific to clade V.

Similarly, filarial worms have one-to-one homologs of *tax-4* (α-type) and *tax-2* (β-type) CNG channel subunits, but lack *cng-1* and *cng-3* (Figure 3B/D/F, S3 Data). Filarial worm genomes possess a third CNG (Bm7148) that is related to both *cng-2* and *che-6*, but phylogenetic analysis suggests the divergence of *cng-2* and *che-6* to have occurred later than the most recent common ancestor of the Filarioidea and *C. elegans*, making it difficult to ascribe putative function to the *cng-2/che-6* homolog in Filarioidea. In *C. elegans*, TAX-2 and TAX-4 are broadly expressed and mediate both thermosensory and chemosensory function, while other CNG channels with more restricted expression patterns have been shown to modulate these pathways (53). It is unclear whether *Bm*-TAX-4 and *Bm*-TAX-2 coordinate different sensory modalities as in *C. elegans*, or if Bm7148 interacts with these proteins and pathways.

Treatment with a nematode TRPV agonist inhibits chemoattraction but not chemoaversion of infective-stage Brugia *larvae*

Our bioinformatic analyses show that filarial worms have evolved divergent sets of chemoreceptors, but maintain much of the core structure of the chemosensory pathway as modeled in *C. elegans*. To test conservation of chemosensory function in filarial worms TRPV channels, we treated infective-stage *Brugia* L3s with nicotinamide (NAM), an agonist of the *C. elegans* OSM-9/OCR-4 heteromeric channel (54), and measured chemotactic responses to host-associated cues. These experiments were performed with *Brugia pahangi*, a model *Brugia* species (21,22,24). *B. pahangi* L3s freshly extracted from infected *Aedes aegypti* are strongly attracted to both fetal bovine serum (FBS) and sodium chloride but are weakly repulsed by 3-methyl-1-butanol (a component of human sweat attractive to *Strongyloides stercoralis* and *Anopheles gambiae*) (8,13,49) (Figure 4A). Treatment of freshly extracted L3s with 250 μM NAM significantly reduced chemoattraction to serum (45.2% reduction) and sodium chloride (61.7% reduction), but had no significant effect on aversion to 3-methyl-1-butanol. NAM-treatment did not impact worms' overall translational movement on the chemotaxis plates (Figure 4B), indicating that NAM causes a specific chemotaxis defect rather than a general depression in movement ability.

To ensure the *Bp-osm-9*, the putative target of NAM, was expressed during the performance window of our assay and that expression was not altered by the ambient temperatures that L3s experience during assay preparation, we measured the relative expression of *Bp-osm-9* in L3s immediately after extraction from mosquitoes, and after 4 hours of *in vitro* culture at human body temperature (37°C) or ambient temperature (21°C). The relative expression of *Bp-osm-9* was unchanged over this time frame at either temperature (p = 0.4215, Figure 4C).

Although the expression of *Bp-osm-9* does not drastically change following extraction, parasites maintained overnight under standard culture conditions do not show a chemotactic response to serum, even with pre-assay incubation in serum-free media (Figure 4D), and show a reduced motility on the chemotaxis plate when compared to untreated freshly extracted parasites. Although it is possible that the specific unknown chemoreceptors involved in serum response are downregulated by this time point, it is more likely that artificial culture conditions have effects on parasite health that compromise chemotactic potential. These results highlight the importance of using freshly extracted L3 larvae in these assays.

Treatment with a nematode TRPV agonist alters infective-stage Brugia *larvae thermosensory response*

L3-stage larvae that have departed the intermediate mosquito host are challenged with stark temperature shifts from the ambient temperature in the mosquito, to warmer temperatures on the definitive host's skin ~24-34°C (55), to a warmer still intra-host core temperature of 37°C. During *in vitro* culture, healthy L3 worms elongate and vigorously thrash in media (Figure 5A), but thrashing will transition to coiling and reduced motility as culture media cools (Figure 5B). In the course of performing L3 chemotaxis experiments with NAM, we noticed that treated L3s had a reduced coiling response. To confirm this effect, we performed dose-response experiments and video-recorded parasites exactly 20 minutes after transfer from 37°C to room temperature, at the point where untreated parasites tightly coil. Blinded scoring of larval coiling reveals that NAM inhibits this thermosensory response in a dose-dependent manner after 24 and 48 hours (Figure 5C-D). These data suggest that OSM-9 plays a polymodal sensory role in *Brugia* L3 stage parasites, potentially mediating both chemosensory and thermosensory responses.

Pretreatment of microfilariae with NAM reduces L3 burden in infected mosquitoes and alters tissue distribution

Assays with extracted L3s indicated that Bp-OSM-9 may be important for *in vitro* chemoattraction to salt and serum. We hypothesized that NAM could dysregulate intra-mosquito chemotaxis of larval stages *in vivo*. To establish an assay to test this hypothesis, we first investigated whether NAM had any effect on mosquito blood-feeding dynamics. When NAM was added to blood and provided to mosquitoes to feed *ad libitum*, 0.1 µM to 5 mM NAM acted as a phagostimulant, causing a dose-dependent increase in the proportion of mosquitoes that had fed after 30 minutes. However, feeding proportions decreased at concentrations greater than 5 mM, and 250 mM NAM caused complete repulsion to the blood (Figure 6A). We chose 5 mM and 25 mM as initial treatment concentrations for mf, and with replication we found that 5 mM NAM caused a significant increase in the proportion of mosquitoes that fed, while 25 mM caused no significant difference from unsupplemented blood (Figure 6B). To ensure that the increase in proportion of fed mosquitoes was not correlated to an increased blood meal size, we measured distended abdomens of mosquitoes after feeding on control blood or blood supplemented with 5 mM or 25 mM NAM (S3 Figure). Mosquito abdomen sizes were unchanged by NAM supplementation, assuring that altered parasite burdens after feeding would not be a function of altered numbers of ingested mf (Figure 6C).

We next supplemented microfilaremic blood with 5 mM and 25 mM NAM and tested for altered infectivity and intra-mosquito tissue distribution of larvae. Pretreatment with NAM of *B. pahangi* mf caused a significant, dose-dependent reduction in parasite burden at 14 DPI (Figure 6D-E, 5 mM = 21% reduction, 25 mM = 43% reduction) and a significant decrease in the proportion of L3s recovered in the thorax of

infected mosquitoes (Figure 6F). The proportion of L3s recovered in the thorax was not correlated to total L3s recovered per mosquito (S4 Figure), suggesting that changes in larval infectivity were not due to differences in blood meal size, but instead the specific action of NAM upon the parasite. Thus, we postulate that NAM inhibits the initial migration of mf from the blood bolus, but that once across (and relieved of NAM exposure in the midgut), developed L3 larval parasites are able to migrate to the head at the same proportion as untreated controls.

Bp-osm-9 and Bp-tax-4 RNAi inhibits chemoattraction of infective-stage larvae toward host-associated cues

NAM is an agonist of the *C. elegans* TRPV heteromer OSM-9/OCR-4 and *Drosophila* orthologs Nanchung/Inactive when expressed in *Xenopus* oocytes, but not of either *C. elegans* subunit alone (54). Given conservation of NAM-receptor interactions across these phyla, we expect *Brugia* OSM-9 orthologs to also respond to NAM. However, the pharmacology and subunit interactions of *Brugia* OSM-9 may differ (e.g., filarial parasites do not have a homolog of *ocr-4* (Figure 3A)), and NAM is an endogenous metabolite in *C. elegans* that has pleiotropic effects (54,56–60). This compelled us to use a genetic approach to more directly test whether *Brugia* OSM-9 and TAX-4 are involved in parasite chemotaxis behavior.

We carried out intra-mosquito RNA interference (RNAi) (61) of both *Bp-osm-9* and *Bp-tax-4* in larval stages and measured the effects on L3 *in vitro* chemotaxis. Infected mosquitoes were injected with dsRNA targeting transcripts of interest at 9 DPI, corresponding to the expected timeline of L2 to L3 transition in the thoracic musculature (8) (Figure 7A). We attempted to confirm knockdown of target transcripts with qPCR, but the low target abundance of *bp-osm-9* and *bp-tax-4* relative to housekeeping genes, coupled with limited recovery of RNA from a small number of assayed parasites prevented reliable amplification. Targeting either *bp-osm-9* or *bp-tax-4* using the '*in squito*' RNAi protocol resulted in the inhibition of *B. pahangi* L3 *in vitro* chemotaxis towards serum at 14 DPI (Figure 7B), while injection of non-specific (*lacZ*) dsRNA had no effect on chemotaxis (control chemotaxis index (CI): 0.83, *bp-osm-9(RNAi)* CI: 0.21, *bp-tax-4(RNAi)* CI: 0.12). dsRNA treatment did not have any effect on general parasite motility on the assay plate (Figure 6C). To our knowledge, this is the first time that either *tax-4* or *osm-9* have been shown to have a specific function in chemosensation in a parasitic nematode.

Bm-osm-9 and Bm-tax-4 do not rescue chemotaxis defects in C. elegans

To further explore the chemosensory function of *Brugia osm-9* and *tax-4*, we tested whether these genes could rescue loss-of-function of orthologous genes in *C. elegans*. While the sequenced genome of *B. malayi* is near completion, many of the gene models remain fragmented and unconfirmed, so we performed low-pass PacBio isoform sequencing with long-read RNA-seq on *B. malayi* adult males and females. This led to the successful capture of *Bm-osm-9* full-length transcripts, but failed to capture *Bm-tax-4*. Using these data and the predicted gene model of *Bm-tax-4*, we cloned these genes and expressed them in the corresponding loss-of-function *C. elegans* backgrounds (*osm-9(ky10), tax-4(p678)*) (27,29) using *Ce-osm-9* and *Ce-tax-4* promoter regions. The *bm-osm-9* clone, along with the two full length isoforms captured by long-read sequencing, included a 41 bp insertion that corresponded to a missing splice-acceptor site at intron 17 that was not reflected in the original gene prediction (S5 Figure). This insertion caused a frame-shift in the predicted amino acid sequence that made the resulting sequence more similar to the *Ce-osm-9* sequence than the original prediction (S6 Figure). The consensus *bm-tax-4* transcript we cloned had two differences from the predicted model(35), a synonymous 694T>C

that was found in 4 out of 7 sequenced clones, and a 21 bp deletion that was found in all clones and corresponds to a mispredicted splice-donor site at intron 2 (S7 Figure). We used these clones to carry out population chemotaxis experiments to test for rescue of *C. elegans* chemotaxis defects by the *B. malayi* homologs.

Bm-osm-9 and *Bm-tax-4* did not rescue chemotaxis defects to diacetyl and isoamyl alcohol, respectively (Figure 8). Heterologous expression of parasitic nematode genes in *C. elegans* genes has been used in the past, with varying success (62–66). In *C. elegans*, both OSM-9 and TAX-4 likely operate in heteromeric channels and are interdependent upon OCR-2 and TAX-2, respectively, for ciliary trafficking within amphid neurons (30,67) and TAX-4 and TAX-2 form a functional heteromeric channel when heterologously expressed (68). It is possible that *Bm-osm-9* and *Bm-tax-4* are unable to form functional complexes in *C. elegans* through interactions with native subunits. It is unclear whether these parasite proteins require co-expression of other parasite subunits to function, whether additional protein-protein interactions are necessary for proper membrane trafficking or regulation, or whether Bm-OSM-9 and Bm-TAX-4 have distinct functions that are unable to be recapitulated in *C. elegans*.

Discussion

Filarial worms continue to pose a significant threat to human and animal health. The ability for filarial worms to move through and between hosts relies on their ability to sense their environment, evidenced by the diversity of genus-specific niches occupied by different filariae when they migrate within shared arthropod or vertebrate hosts (e.g. *Brugia* larvae migrate to the thoracic musculature of *Ae. aegypti*, while *Dirofilaria* migrate to the Malphigian tubules). Despite the importance of sensory behaviors in the evolution and persistence of parasitism, little is known of the receptors and pathways that control such behaviors in parasitic nematodes. Identifying mediators of sensory-associated behaviors can aid our understanding of disease transmission and pathogenesis, and may also provide new targets for therapeutic intervention.

We have shown that filarial worms have a greatly reduced and divergent set of chemoreceptors as compared to *C. elegans* and the rest of the Nematoda, but that they retain much of the core downstream chemosensory signaling pathway. Filarial parasites exhibit stage, tissue, and sex-specific chemoreceptor patterns that likely correspond to the different vector and host environments encountered throughout the life cycle. We expect that these patterns correspond to landmark migration events, including the migration of larvae within the mosquito host, the transmission of infective larvae (L3s) to the definitive host, the early migration of larvae to the lymphatics, and the potential mate-seeking behaviors of dioecious adults.

Historically, it has been difficult to identify endogenous ligands for nematode chemoreceptors. In *C. elegans*, only a small fraction of chemoreceptors have been linked to activating molecules, some of which are not likely to be the natural ligand (46,69–77). This is partly a function of the large number of chemoreceptors (>1,400) and the large space of potentially relevant terrestrial cues in free-living clade V nematodes. The smaller complement of chemoreceptors in clade IIIc filarial parasites and the overlay of temporal receptor expression patterns with possible host-derived molecules present at intra-host sites of parasite migration, may facilitate a comparatively easier path to chemoreceptor deorphanization. Efforts are underway to develop new heterologous expression platforms for deorphanization that may be more amenable to the expression of nematode GPCRs, which have often been recalcitrant to expression in single-cell mammalian or yeast systems.

As in *C. elegans*, TRP and CNG channels in filarial worms likely function downstream of chemoreceptors expressed on the cilia of sensory amphids. We show that a TRPV chemical agonist inhibits *in vitro* chemotaxis of infective *Brugia* larvae towards host-associated cues and compromises the ability of microfilariae to establish mosquito infections. RNAi experiments implicate both *Brugia* OSM-9 and TAX-4 as necessary for larval chemotaxis to serum. In *C. elegans*, OSM-9 and TAX-4 function as primary sensory transducers in distinct sensory cells that can respond to distinct chemicals. It is interesting that both OSM-9 and TAX-4 mediate responses to serum in *B. pahangi*. FBS is a complex heterogeneous mixture of macromolecules, amino acids, and ions, and it is conceivable that different components of this mixture activate distinct chemoreceptors, chemosensory neurons, and downstream pathways in *Brugia*. Little is known about the neuronal architecture of filarial worms, and it is also possible that OSM-9 and TAX-4 are coexpressed and have homologous function in the same cells. A map of the filarial worm connectome and the ability to produce transcriptional reporters would help resolve this question, and will be hastened by technologies to more easily dissect filarial worm neuroanatomy and neurogenetics (78). Furthermore, fractionation of serum into pure chemicals for chemotaxis experiments could illuminate whether multiple cells are involved in *Brugia* chemotactic responses to serum or other crude preparations.

CNG and TRP channels are polymodal in *C. elegans* and function in sensory neurons responsible for aerosensation, mechanosensation, chemosensation, noxious avoidance, and thermosensation, among others (27–29,79–81). Our data suggests a similar polymodal deployment of these channels in mosquito-borne filarial worms, though the pattern of neuronal expression may differ. While OSM-9 in *C. elegans* is involved in noxious heat avoidance in the nociceptive ASH neuron (80), it is TAX-4 and TAX-2 that function in the sensation of precise of thermal gradients via AFD. Whether filarial worms have cooperative thermal sensory programs is unknown, but given the tight range of temperatures experienced by these parasites (ambient temperatures while in mosquitoes, physiological temperatures in mammalian hosts) and the unlikelihood of experiencing or being able to avoid noxious heat or cold, the sensory program in filarial worms is likely more simple than their free-living counterparts. Our data suggests that OSM-9 is involved in this program, but CNGs like TAX-4/TAX-2 cannot be ruled out.

Questions remain as to the pharmacology and subunit interactions of TRP and CNG channels that function in *Brugia* chemosensation. The inability of *bm-tax-4* or *bm-osm-9* to rescue chemotaxis defects in *C. elegans* knockouts suggest that these heterologously expressed genes are unable to form homomeric channels or heteromeric channels with endogenous *C. elegans* subunits that function in a homologous manner. The clade IIIc loss of CNGs involved in olfactory plasticity (*cng-1*, *cng-3*) and TRPs that are expressed in the mechanosensory labial QLQ neurons of *C. elegans* (*ocr-4*, *trpa-1*) indicate that there is not perfect conservation of all sensory modalities between *C. elegans* and filarial worms, and it is possible that filarial worm TRP and CNG channels have evolved subunit interactions or primary functions that are not conserved in *C. elegans* (30,51,82,83).

Deeper knowledge of chemotaxis has been achieved in clade IV and V nematodes that are more amenable than filarial worms to *in vitro* culture and manipulation (Gang and Hallem 2016; Haas 2003). Continued development of genetic tools (Song et al. 2010; Liu et al. 2018) and sensory assays would help to further elucidate the molecular basis for sensory behaviors in clade III LF parasites. The *in vitro* chemotactic capacity of filarial worm L3s is transitory, and adults, which are healthy in culture much longer than larval parasites, could offer an additional platform for sensory pathway dissection. Exploration of other sensory modalities such as thermosensation and mechanosensation are essential to develop a more thorough model of how filarial worms integrate sensory data in order to successfully invade, infect, and migrate within the host.

Materials and Methods

Protocol and data availability

All comparative genomics, phylogenetics, data analysis, and data visualization pipelines are publicly available at https://github.com/zamanianlab/BrugiaChemo-ms. Short-read and long-read sequencing data has been deposited into NIH BioProjects PRJNA548881 and PRJNA548902, respectively.

Parasite and mosquito maintenance

Microfilariae (mf), L3, and adult stage FR3 strains of *Brugia malayi* and *Brugia pahangi* from the NIH/NIAID Filariasis Research Reagent Resource Center (FR3) (Michalski et al. 2011) were maintained in RPMI 1640 culture media (Sigma-Aldrich, St. Louis, MO) with penicillin / streptomycin (0.1 mg/mL, Gibco, Gaithersburg, MD) and FBS (10% v/v, Gibco) unless otherwise stated. For local production of L3 stage *B. pahangi,* mf were incubated in defibrinated sheep's blood (Hemostat, Dixon, CA) at a density of 120-160 mf / 20 µl at 37ºC in a membrane feeder(85). mf were exposed to groups of 250 adult female *Aedes aegypti* Liverpool strain (LVP) 1-3 day post-emergence starved 1 day prior to feeding. Infected mosquitoes were maintained in double housed cages in a Percival Scientific incubator (Perry, IA) model I-36NL incubator (26°C, 85% humidity, 12:12 hr light:dark cycle) and provided 10% sucrose throughout.

At 14 days post-infection (DPI) L3 stage parasites were extracted into warm *Aedes* saline (86) or RPMI 1640 (Sigma-Aldrich) via micro-dissection of cold anesthetized mosquitoes or bulk isolation as previously described(9). The prevalence and locality of L3s was determined by separating head, thorax, and abdominal tissues during dissection with all L3s counted per mosquito. *B. malayi* adults used for RNA-seq were received from the FR3 and were immediately washed and placed in new media. Adult parasites were allowed to equilibrate at 37°C for 24 hours before any further experimentation.

Caenorhabditis elegans *strains*

C. elegans strains were maintained at 20°C on NGM plates seeded with *E. coli* strain OP50 and routinely picked to fresh plates at the L4 stage. Transgenic strains were created as described(87) by microinjecting 50 ng/uL of parasite transgene, combined with either unc-122p::GFP or myo-2p::GFP as co-injection markers and an empty vector to achieve a final concentration of 100 ng/uL. Genotypes used include: *osm-9(ky10)* IV, *tax-4(p678)* III*,* ZAM13: *osm-9(ky10)* IV, *mazEx13*[*osm-9p::bm-osm-9::unc-54* 3'UTR*; unc-122p::GFP*], ZAM14: *tax-4(p678)* III, *mazEx14 [tax-4p::bm-tax-4::unc-54* 3'UTR*; myo-2p::GFP]*.

Comparative genomics

Chemosensory GPCRs: The chemoreceptor mining and annotation strategy is charted in S1 Figure. Briefly, all filarial worm predicted proteomes in WormBase ParaSite version 9(35) and a selected list of high-quality genomes that included representatives from the four major nematode clades (39 total species, S1 Table) were searched (hmmsearch(88)) against a database of profile hidden Markov models (HMMs) curated by Pfam, consisting of primary metazoan GPCR families and the nematode chemoreceptor families(89). Predicted proteins were filtered such that each that had a best-hit to a nematode chemoreceptor HMM was retained. Surviving predicted proteins were then used in a reciprocal

search (hmmsearch) against the entire Pfam HMM database. Predicted proteins that had a best-hit to a nematode chemoreceptor HMM were retained. Surviving predicted proteins were then searched (blastp(90)) against the *C. elegans* predicted proteome (N2, WBPS9), and predicted proteins that had a best-hit to a *C. elegans* chemoreceptor (S4 Data) were retained (*C. elegans* chemoreceptors were obtained by downloading all named chemoreceptors from WormBase and their paralogues via the WormBase ParaSite API).

TRP and CNG receptors: Predicted protein sequences of annotated TRP and CNG channels from *C. elegans* were downloaded from WormBase(91) and used as seeds in blastp searches against all predicted proteomes included in S1 Table. Hits with an E-value < 0.01 were reciprocally searched against the *C. elegans* predicted proteome, and any hit that wasn't most similar to a *C. elegans* TRP or CNG channel was removed. Because there were clade and species-specific gene losses in the CNG family, *C. elegans* seeds were also used in a tblastn search against parasite genomes to account for missing gene models and possible errors in gene predictions.

Phylogenetics

Chemosensory GPCRs: Predicted protein sequences belonging to *C. elegans* chemoreceptor families (37) were aligned by family with MAFFT(92). The resulting family profile HMMs were sequentially aligned with MUSCLE(93) to create a master *C. elegans* chemoreceptor alignment. Predicted chemoreceptors from 19 selected species underwent transmembrane domain prediction with HMMTOP(94), and only those that contained exactly 7 predicted TMs were aligned to the master alignment. This final multiple sequence alignment was trimmed with trimAl(95) such that columns with greater than 30% gaps were removed, and sequences that did not have at least 70% of residues that aligned to columns supported by 70% of the sequences were removed.

The trimmed, filtered alignment was subjected to maximum-likelihood phylogenetic inference with IQ-TREE(96) and ModelFinder(97) with ultrafast bootstrapping(98), using the VT substitution matrix(99) with empirical base frequencies and a free-rate substitution model(100,101) with 10 categories. Bootstrap values from 1000 replicates were drawn as nodal support onto the maximum-likelihood tree.

TRP and CNG receptors: Putative TRP sequences underwent TM prediction, and any sequences with ≥1 predicted TMs were retained. TRP and CNG sequences were separately aligned, trimmed such that columns with greater than 25% gaps were removed, and CNG sequences that did not have at least 70% of residues that aligned columns supported by 70% of the sequences were removed. For both datasets, fragments with large gaps or putative isoforms were manually removed. Alignments were subjected to Bayesian phylogenetic inference with MrBayes(102). The MCMC chain was run for 10,000,000 generations, with a sample taken every 1000 generations. Eight separate chains were run, with two hot chains and the temperature set to 0.05. Consensus trees were drawn using the 50% majority rule, with all compatible groups added, and posterior probabilities were drawn as nodal support. All trees were annotated with ggtree(103).

Brugia malayi *transcriptomic analyses*

Anterior and posterior *B. malayi* transcripts: One millimeter of the anterior and posterior ends of adult male and female *B. malayi* were cut from live parasites and immediately transferred to Trizol (Ambion, Waltham, MA). Tissue in Trizol was homogenized with a plastic pestle, and RNA was extracted with

Direct-zol RNA miniprep kit (Zymo, Irvine, California) according to the manufacturer's instructions and was eluted in RNase-free water. RNA was DNase-treated on the column, and the quality of purified RNA was assessed with Qubit (Thermo Fisher Scientific, Waltham, MA) and Bioanalyzer Pico chip (Agilent, Santa Clara, CA). RNA was rRNA depleted with Ribo-Zero ScriptSeq Complete Gold (Blood) (Illumina, San Diego, CA) and sequencing libraries were constructed using the TruSeq Stranded Total RNA kit (Illumina). All samples were sequenced at the UW-Madison Biotechnology Center with an Illumina HiSeq 2500 with a single-end 100 bp read setting. Reads were adapter and quality trimmed using Trimmomatic(104). HiSAT2(105) and StringTie(106) were used to align reads to the *B. malayi* reference genome (WormBase ParaSite(35), release 12 version 4) and to produce TPM (transcripts per million) counts for annotated genes. The RNA-seq pipeline was implemented using Nextflow(107) and is publicly available (https://github.com/zamanianlab/Bmalayi_HTRNAseq-nf). Custom R scripts were used for profiling, hierarchical clustering, and visualization of putative chemosensory gene expression across anterior and posterior samples.

Stage-specific expression of *B. malayi* chemosensory genes: Public stage-specific RNA-seq data(49) was acquired from NCBI SRA. Reads were aligned to version 4 of the *B. malayi* genome, downloaded from version 12 of WormBase ParaSite(35). Reads were aligned with HISAT2(105) and StringTie(106). Custom R scripts were used for profiling, hierarchical clustering, and visualization of putative chemosensory gene expression across life stages. Heatmaps of life stage expression were drawn according to chromosomal location. The RNA-seq pipeline was implemented using Nextflow(107) and is publicly available (https://github.com/zamanianlab/BmalayiRNAseq-nf). Locus information was extracted from GTF files from WormBase ParaSite(35) and plots were generated with Circos(108).

Brugia *chemotaxis assays*

All chemotaxis assays were performed immediately after extraction of L3s from local infections and following previously published protocols(22–24). For nicotinamide (NAM, DOT Scientific, Burton, MI) treatment experiments, extracted parasites were first sorted from warm RPMI 1640 into room temperature RPMI 1640, and half of the parasites were placed in media supplemented with a final concentration of 250 μM NAM and incubated for 30 min. Heat-inactivated FBS (Gibco), 1 M NaCl (Thermo Fisher Scientific), and 1:1 3-methyl-1-butanol (Thermo Fisher Scientific) in mineral oil were used as cues. A curved platinum worm pick was used to remove L3s from warm media and place them on 0.8% agarose plates, plates were transferred to a 37°C incubator with 5% atmospheric CO_2, and parasites were allowed to migrate for 30 minutes after which the plates were removed and scored. The chemotaxis index (CI) of each plate was calculated as follows: CI = (T - C) / (T + C + O), where T is the number of parasites that have migrated to the test cue, C is the number that migrate to the control cue, and O is the number that have migrated outside of the designated cue areas. To account for parasite injury in transfer, only plates that had C + T > 2 were used for statistical analysis and plotting.

Larval coiling assay

NAM treatment of *B. pahangi* L3 was performed with parasites from in-house infections or received from the FR3. After extraction or receipt, parasites were washed with fresh RPMI and suspended in complete media (RPMI 1640 + 10% FBS + penicillin/streptomycin) at a density of 1 parasite per 2 μL. A 96-well plate was arranged with 50 μL of complete media with 2X NAM in each well, with 4-5 wells as technical replicates for each NAM concentration. Parasites were pipetted into each individual well to create a density of 10-25 parasites per well in a final volume of 100 μL. Plates were immediately transferred to a

37°C incubator with 5% atmospheric CO_2 and were left untouched until videos were recorded at 24 and 48 hours post-treatment. Care was taken not to disturb parasites while transferring the plates from the incubator to the recording stage. Parasites were allowed to cool at room temperature for 20 min. on the recording stage, after which each well was recorded for 10 s. at 16 FPS. Recording was performed at 2.5X on a Zeiss Stemi 508 with a K LAB stand and oblique light with a monochrome CMOS camera (DMK 33UX178, The Imaging Source). Parasites were returned to the incubator after recording.

Videos were assigned randomized file names and distributed to 3 researchers for manual scoring of coiling. Researchers blindly rated each well on a scale of 0-5 where 0 is the most coiling and 5 is the least coiling. Scores were collated and data was blindly analyzed and plotted with the tidyverse package(109) and custom R scripts.

Aedes aegypti *feeding and engorgement assays*

3-4 day old adult female *Ae. aegypti* LVP were starved for 24 hours then provided with a blood meal for 30 minutes via a glass membrane feeder (n = 25-50) (Rutledge et al. 1964). Immediately after feeding, groups were cold anesthetized and visually inspected for distended abdomens to measure the proportion of feeding mosquitoes. Blood meal size was measured by calculating the ratio of the mosquito length (abdomen tip to thorax) to width (dorso-ventral width at the 5th abdominal segment) using Fiji (110)(S3 Figure).

Larval temperature-shift assay and qPCR

B. pahangi L3s were extracted in bulk and separated into three treatment treatment groups: immediate storage in Trizol LS (Ambion); 1 mL RPMI 1640 + 10% FBS + penicillin/streptomycin at room temperature; or 1 mL RPMI 1640 + 10% FBS + penicillin/streptomycin in a 37°C heat block. Parasites were incubated in media for 4 hours. After incubation, media was removed, parasites were washed once in fresh RPMI 1640 and stored in Trizol LS at -80°C until processing. To extract RNA, samples were thawed on ice, and the volume was adjusted to a final ratio of 3 Trizol LS : 1 RNase-free water. Samples were lysed with a TissueLyser LT (Qiagen, Venlo, The Netherlands). One 5 mm stainless steel bead was added to each tube, which then underwent two cycles of 3 minutes of shaking at 30 Hz. Tubes were cooled on ice for 2 minutes in between cycles. RNA was extracted with the Direct-zol RNA miniprep kit (Zymo) according to the manufacturer's instructions, including an on-column DNase treatment, and RNA was eluted in 15 µL RNase-free water. RNA samples were quantified with a NanoDrop 1000 and immediately used for first-strand cDNA synthesis with SuperScript III (Thermo Fisher Scientific) using random hexamers and normalizing RNA input. cDNA was stored at -20°C until further use.

For qPCR, GAPDH control primers(111) and *osm-9* primers (designed with Primer3(112), F: CCCGCTGATCCAAACATTG, R: TGCACTACACGTCATATCACTG) were optimized with *B. pahangi* L3 RNA from the FR3 with cDNA synthesized using the same SuperScript III master mix as the experimental RNA samples. A 20 µL reaction was used with 2X PowerUp SYBR Green MasterMix (Thermo Fisher Scientific), 800 nM primers, and 5.2 ng RNA. Reactions were run in duplicate on a StepOnePlus real-time PCR system (Applied Biosystems, Waltham, Massachusetts). C_T values were calculated with the system's automatic threshold, and relative expression was calculated with the $\Delta\Delta C_T$ method(113).

In squito *exposure of infective larva to bp-osm-9 and bp-tax-4 dsRNAs*

Primers were designed to amplify 200-600 bp regions from cloned *bm-tax-4* and *bm-osm-9* which had >95% identity with their *B. pahangi* orthologs, and T7 recognition sequences were appended to the 5' end of each primer. Cloned genes (below) were used as template DNA for PCRs with Phusion polymerase (New England Biolabs, Ipswich, MA). Complete dsRNA synthesis protocols, including primer sequences and thermocycler programs, can be found in S2 File. PCR product was cleaned (Qiagen MinElute PCR Purification Kit) and resuspended in water at a desired concentration of 1-2 ug/uL as measured by a Qubit 3.0 dsDNA assay (Thermo Fisher Scientific). This product was subsequently used as the template for a dsRNA synthesis reaction (MegaScript RNAi, Thermo Fisher Scientific). dsRNA was DNase treated, purified with phenol/chloroform, and resuspended in nuclease-free water at a concentration of 1-4 ug/uL. The concentrations and purity of 1:20 dilutions of dsRNA were measured with a NanoDrop 1000 (Thermo Fisher Scientific).

Ae. aegypti LVP were infected with *B. pahangi* mf as described above. Injections of dsRNA were carried out with the following modifications of an established protocol (61). Prior to injection, infected mosquitoes were starved by removing sucrose pads 8 DPI. At 9 DPI, infected mosquitoes were injected with 250 µL of 1 ug/uL dsRNA, coinciding with the L2 to L3 molt in the thoracic musculature(8). Mosquitoes were injected in cohorts of 25, and cohorts were immediately returned to 26°C and sucrose pads were replaced. Dead mosquitoes were removed daily until time of assay at 14 DPI, at which point mosquitoes were dissected to extract L3s for use in chemotaxis assays.

Long-read sequencing in Brugia malayi *adult males and females*

Total RNA from *B. malayi* adult males and females was obtained from the FR3. RNA quality was assessed by 2100 Bioanalyzer, converted to single stranded cDNA and amplified using the SMARTer PCR cDNA Synthesis Kit (Takara Bio, Kusatsu, Japan), and IsoSeq libraries were constructed with equimolar cDNA fractions (0.5X and 1X) with the SMRTbell Template Prep Kit 1.0 (Pacific Biosciences, Menlo Park, CA). Library quantity and quality were assessed by Qubit HS DNA (Thermo Fisher Scientific) and 2100 Bioanalyzer. Isoforms were clustered and polished from subreads with IsoSeq2, visualized with IGV(114), and annotated with BLAST(115).

Bm-osm-9 and bm-tax-4 cloning

Primers directed toward the ATG start and stop codon of the IsoSeq-generated gene model of *bm-osm-9* and the predicted gene model of *bm-tax-4* were designed with Primer3(112). A full length amplicon was produced with Phusion polymerase (New England Biolabs). Amplicons were A-tailed with GoTaq Flexi (Promega, Madison, WI) and cloned into pGEM-T in JM109 competent cells (Promega). *C. elegans* N2 genomic DNA was extracted with the Qiagen DNeasy kit. A ~1.6 kb portion upstream of *Ce-osm-9*(29) and a ~3 kb portion upstream of *Ce-tax-4*(27) were amplified and cloned into pGEM-T as above. Final expression constructs were assembled with the HiFi Assembly kit (New England Biolabs), using amplicons from the promoter and gene as two fragments, and pPD95.75 (a gift from Andrew Fire (Addgene plasmid # 1494 ; http://n2t.net/addgene:1494 ; RRID:Addgene_1494)) double-digested with XbaI and EcoRI, as the backbone. Complete cloning protocols, including primer sequences and thermocycler programs, can be found in S1 File. All products were verified with Sanger sequencing.

pMZ0019 (*osm-9p::bm-osm-9*), pMZ0020 (*tax-4p::bm-tax-4*) were injected into *C. elegans* hermaphrodites as described and transgenic strains were used for rescue experiments.

Caenorhabditis elegans *chemotaxis assays*

Chemotaxis assays were performed as described(116). For each strain, five L4 worms were picked to each of five seeded NGM plates 4-6 days before the assay date. On assay day, worms were washed off plates and pooled with M9, washed with M9 three times and once with water. For each of five 10 cm chemotaxis plates (2% agar, 5 mM KH_2PO_4/K_2HPO_4 pH 6.0, 1 mM $CaCl_2$ and 1 mM $MgSO_4$) per strain, 1 µL of 1 M sodium azide was place on opposite sides of the plate and allowed to soak in with the plate lids removed. Once dry, 1 µL of cue and diluent were then placed at the same location as the sodium azide. 1:1000 diacetyl (Santa Cruz Biotechnology, Santa Cruz, CA) and 1:10 isoamyl alcohol (Thermo Fisher Scientific) in ethanol were used as cues for the *osm-9* and *tax-4* experiments, respectively. After the addition of cues, 100-200 worms were quickly pipetted to the center of assay plates. Excess water was removed with a Kimwipe (Kimberly-Clark, Irving, TX), and worms were gently spread with a platinum worm pick. Plates were left untouched on a benchtop for 30 minutes at room temperature (~21°C), after which paralyzed animals were counted in total and at each cue and control region. The chemotaxis index (CI) of each plate was calculated as follows: $CI = (T - C) / (T + C + O)$, where T is the number of worms that have migrated to the test cue, C is the number at the control, and O is the number that have migrated to neither the test nor the cue.

Acknowledgements

Figure Captions

Figure 1.

The genomes of filarial worms contain a reduced complement of divergent chemoreceptors. Chemoreceptors were mined from 39 nematode genomes, and the phylogeny of chemoreceptors from a down-sampled species set was constructed with maximum-likelihood (ML) inference. **(A)** Family and superfamily categorizations were used to annotate the final phylogeny. Clade IIIc chemoreceptors are diverged from *C. elegans* and other nematode chemoreceptors, without any one-to-one homologs. Filarial chemoreceptors are notably diverged in *srsx*, *srab*, and *srx*. Nodal values represent bootstrap support of 1000 separate bootstrap replicates. **(B)** Filarial worm genomes contain far fewer chemoreceptors than other parasitic and free-living nematodes, and they are enriched for *srsx*, *srab*, and *srx* receptors. Each box in the heatmap is normalized to the total number of chemoreceptors per species. **(C)** A decrease in

chemoreceptor count is correlated with an increase in extra-host (e.g., terrestrial) stages within nematode life cycles. Completely free-living nematodes such as *C. elegans*, *C. briggsae, P. pacificus*, and *P. redivivus* have many more chemoreceptors than parasitic nematodes that are vector-transmitted or host-contained such as the filarial worms and *T. spiralis*. Values from the bar plot in B are log2 transformed. ρ was calculated with Spearman's rank correlation with the null hypothesis that $\rho = 0$.

Figure 2.

Chemoreceptors are clustered in the *Brugia malayi* genome and are enriched in specific life stages and adult tissues. (A) The chromosomal location of annotated *B. malayi* and *C. elegans* chemoreceptor genes are shown. *C. elegans* chemoreceptors are found throughout the genome but are heavily clustered on chromosome V, and these clusters are typically enriched for specific families and superfamilies(37). Likewise, *B. malayi* chemoreceptors are clustered on chromosomes II and IV. Expression data (purple inner heatmaps) reveal distinct patterns of chemoreceptor expression across the life cycle. **(B)** The anterior 1 mm of adult male and female *B. malayi*, and the posterior 1 mm of males, were isolated and subjected to RNA-seq. Transcripts are clustered by expression pattern across the three samples.

Figure 3.

Filarial worms possess unique complements of broadly conserved nematode TRP and CNG channels. The phylogenies of **(A)** TRP and **(B)** CNG channels were constructed with Bayesian inference. Nodal values represent the posterior probability. **(C)** *osm-9* and **(E)** *ocr-1/2* subtrees were drawn from A, and **(D)** *tax-4* and **(F)** *tax-2* subtrees were drawn from B. Filarial worms have one-to-one orthologs of *C. elegans osm-9*, *tax-4*, and *tax-2*. In contrast, the two *ocr-1/2*-like genes from filarial worms are more closely related to each other than with the homologous *Ce-ocr-1* and *Ce-ocr-2*, and belong to a diverged clade IIIc grouping of OCR-1/2-like channel subunits.

Figure 4.

Treatment with a TRVP agonist dysregulates chemotaxis of *Brugia pahangi* infective larvae. (A) L3 stage parasites were extracted from mosquitoes and subjected to chemotaxis assays with or without 250 µM nicotinamide (NAM) treatment. **(B)** NAM dysregulates attraction of freshly extracted L3s to serum and NaCl, but has no effect on aversion to 3-methyl-1-butanol. **(C)** NAM has no effect on gross translational movement of freshly extracted L3s. **(D)** *Bp-osm-9* expression is unchanged by *in vitro* culture at physiological or room temperature 4 hours post-extraction (HPE). **(E)** L3s cultured for 1-day post-extraction (DPE) do not show chemotaxis toward serum and have reduced motility on the chemotaxis plate when compared to untreated freshly extracted parasites (p = 0.028, t-test). Data for A-C represent the combined results of three independent biological replicates, except for the experiments with 3-methyl-1-butanol, which included two replicates (cohorts of mosquito infections). Data for D represents the results of two biological replicates. Each point represents a single chemotaxis plate with 8-10 L3s. Red diamonds and bars indicate the mean and standard error of the mean. Comparisons of means were performed using t-tests (**: p <= 0.01).

Figure 5.

Treatment with a TRPV agonist impairs the temperature-shift coiling response in *Brugia pahangi* infective larvae

(A) L3 stage parasites were extracted from mosquitoes and treated with NAM, subjected to a temperature shift, and analyzed for cooling-induced coiling behaviors. (B) Representative images of untreated (control) individuals displaying the coiled phenotype and 1 mM NAM exposed individuals with uncoiled thrashing. (C) Blinded coiling score given to each treatment after 24 hours and 48 hours post-treatment. Red diamonds and bars indicate the mean and standard error of the mean from three biological replicates, each composed of >3 technical replicates and scored by three different researchers. Comparisons of means were performed using t-tests. (*: $p <= 0.05$; **: $p <= 0.01$, ***: $p <= 0.001$; ****: $p <= 0.0001$)

Figure 6.

Treatment with a TRPV agonist reduces the ability of microfilariae to establish infection in mosquitoes. (A) Nicotinamide (NAM) added to blood at up to 50 mM increases the proportion of blood-fed mosquitoes when allowed to feed to repletion, but reduces mosquito blood-feeding at concentrations greater than 5 mM. Black points represent technical replicates and grey diamonds represent the mean. **(B)** Replication of blood-feeding experiments with 5 mM and 25 mM showed a significant increase in the proportion of blood-fed mosquitoes when blood was supplemented with 5 mM NAM, but no difference when supplemented with 25 mM. These concentrations were used for subsequent parasite treatment. Points represent the values from three independent biological replicates (cohorts of mosquitoes). **(C)** Blood supplemented with 5 or 25 mM NAM does not alter the size of distended mosquito abdomens after blood-feeding, indicating an unaltered size of blood meal. Points represents the measured abdomens of individual mosquitoes from a single blood-feeding experiment. **(D-E)** Pre-treatment of *B. pahangi* microfilaria (mf) with NAM prior to mosquito infection causes a dose-dependent reduction in the number of L3s recovered per mosquito. P-values were calculated with Tukey's post-hoc tests and adjusted for multiple comparisons. **(F)** Reduction in L3 recovery was due to a decrease in larval parasites in the mosquito thorax (i.e. the flight muscles, the migratory destination for mf and site of development for L1, L2, and early-L3 stage parasites). Data from D-F represents the combined results of three independent biological replicates (cohorts of mosquito infections); each point represents the parasites recovered from an individual mosquito. Red diamonds and bars indicate the mean and standard error of the mean. Comparisons of means in B and F were performed using t-tests. (*: $p <= 0.05$; **: $p <= 0.01$)

Figure 7.

dsRNA treatment of chemosensory pathway receptors causes defective chemotaxis of *Brugia pahangi* infective larvae. (A) Injection of 250 ng dsRNA into *B. pahangi*-infected *Ae. aegypti* LVP was performed 9 DPI, and L3 parasites were recovered via dissection at 14 DPI. Recovered parasites were immediately used in chemotaxis experiments. Intra-mosquito developmental dynamics adapted from (8). **(B)** dsRNA treatment of *bp-osm-9* or *bp-tax-4* resulted in a reduced ability of L3s to migrate to serum. Control parasites were recovered from mosquitoes injected with *lacZ* dsRNA. dsRNA exposure does not inhibit general translational motility on the chemotaxis plate. Data represents the combined results of three independent biological replicates (cohorts of mosquito infections); each point represents the chemotaxis index of an individual plate. Red diamonds and bars indicate the mean and standard error of the mean. Comparisons of means were performed using t-tests. (***: $p <= 0.001$; ****: $p <= 0.0001$)

Figure 8.

Heterologous expression of *B. malayi* homologs of chemosensory pathway receptors does not rescue loss-of-function chemotaxis defects in *C. elegans*. *B. malayi* genes were cloned and

expressed under the control of the endogenous promoter from their *C. elegans* homologs (27,29), and transgenic *C. elegans* were created by microinjection. **(A)** Chemotaxis defects to diacetyl (OSM-9 functioning through AWA) and **(B)** isoamyl alcohol (TAX-4 functioning through AWC) were not rescued by the *B. malayi* homologs. Data represents the combined results of three independent biological replicates, each consisting of 5 technical replicates; each point represents the chemotaxis index of an individual plate. Red diamonds and bars indicate the mean and standard error of the mean. Comparisons of means were performed using t-tests. (****: p <= 0.0001)

Supporting Information

S1 Table. Spreadsheet of species included in the comparative analysis, clade designation, genome BioProject, and whether or not each species is represented in the trees
S1 Data. Chemoreceptor IQ-TREE consensus tree in Newick format
S2 Data. TRP MrBayes consensus tree in Nexus format
S3 Data. CNG MrBayes consensus tree in Nexus format
S4 Data. List of *C. elegans* chemoreceptors IDs
S1 Figure. Flow chart of comparative genomics pipeline
S2 Figure. Alternative plot of *B. malayi* head/tail RNA-seq
S3 Figure. Representative images of measured mosquito abdomens
S4 Figure. L3 recovery correlation plot
S5 Figure. osm-9 nucleotide alignment
S6 Figure. osm-9 amino acid alignment, including Inactive from *Drosophila melanogaster*
S7 Figure. tax-4 amino acid alignment
S1 File. List of all identified chemoreceptors with family and superfamily annotations
S2 File. Complete protocols for all cloning efforts

1. James SL, Abate D, Abate KH, Abay SM, Abbafati C, Abbasi N, et al. Global, regional, and national incidence, prevalence, and years lived with disability for 354 diseases and injuries for 195 countries and territories, 1990–2017: a systematic analysis for the Global Burden of Disease Study 2017. Lancet. 2018 Nov 10;392(10159):1789–858.

2. Krishna Kumari A, Harichandrakumar KT, Das LK, Krishnamoorthy K. Physical and psychosocial burden due to lymphatic filariasis as perceived by patients and medical experts. Trop Med Int Health. 2005 Jun;10(6):567–73.

3. Weiss MG. Stigma and the social burden of neglected tropical diseases. PLoS Negl Trop Dis. 2008 May 14;2(5):e237.

4. Ton TGN, Mackenzie C, Molyneux DH. The burden of mental health in lymphatic filariasis. Infect Dis Poverty. 2015 Jul 30;4:34.

5. World Health Organization. Weekly epidemiological record [Internet]. 2018 Nov. Report No.: 44. Available from: https://apps.who.int/iris/bitstream/handle/10665/275719/WER9344.pdf?ua=1

6. King CL, Suamani J, Sanuku N, Cheng Y-C, Satofan S, Mancuso B, et al. A Trial of a Triple-Drug Treatment for Lymphatic Filariasis. N Engl J Med. 2018 Nov 8;379(19):1801–10.

7. Anderson RC, Anderson RC. Nematode Parasites of Vertebrates: Their Development and Transmission. CABI Pub.; 2000. 650 p.

8. Erickson SM, Xi Z, Mayhew GF, Ramirez JL, Aliota MT, Christensen BM, et al. Mosquito infection responses to developing filarial worms. PLoS Negl Trop Dis. 2009 Oct 13;3(10):e529.

9. Lindsay SW. The migration of infective larvae of Brugia pahangi within the mosquito, Aedes aegypti. Parasitology. 1986 Apr;92 (Pt 2):369–78.

10. Denham DA, McGreevy PB. Brugian filariasis: epidemiological and experimental studies. Adv Parasitol. 1977;15:243–309.

11. Bryant AS, Ruiz F, Gang SS, Castelletto ML, Lopez JB, Hallem EA. A Critical Role for Thermosensation in Host Seeking by Skin-Penetrating Nematodes. Curr Biol. 2018 Jul 23;28(14):2338–47.e6.

12. Castelletto ML, Gang SS, Okubo RP, Tselikova AA, Nolan TJ, Platzer EG, et al. Diverse host-seeking behaviors of skin-penetrating nematodes. PLoS Pathog. 2014 Aug;10(8):e1004305.

13. Gang SS, Castelletto ML, Bryant AS, Yang E, Mancuso N, Lopez JB, et al. Targeted mutagenesis in a human-parasitic nematode. PLoS Pathog. 2017 Oct 10;13(10):e1006675.

14. Gang SS, Hallem EA. Mechanisms of host seeking by parasitic nematodes. Mol Biochem Parasitol. 2016 Jul 1;208(1):23–32.

15. Tsubokawa D, Hatta T, Kikuchi T, Maeda H, Mikami F, Alim MA, et al. Venestatin, a Ca++-binding protein from the parasitic nematode Strongyloides venezuelensis, is involved in the larval migration process. Int J Parasitol. 2017 Jul;47(8):501–9.

16. Ruiz F, Castelletto ML, Gang SS, Hallem EA. Experience-dependent olfactory behaviors of the parasitic nematode Heligmosomoides polygyrus. PLoS Pathog. 2017 Nov;13(11):e1006709.

17. Baiocchi T, Lee G, Choe D-H, Dillman AR. Host seeking parasitic nematodes use specific odors to

assess host resources. Sci Rep. 2017 Jul 24;7(1):6270.

18. Dillman AR, Guillermin ML, Lee JH. Olfaction shapes host–parasite interactions in parasitic nematodes. Proceedings of the [Internet]. 2012; Available from: https://www.pnas.org/content/109/35/E2324.short

19. Hallem EA, Dillman AR, Hong AV, Zhang Y, Yano JM, DeMarco SF, et al. A sensory code for host seeking in parasitic nematodes. Curr Biol. 2011 Mar 8;21(5):377–83.

20. Bryant AS, Hallem EA. Terror in the dirt: Sensory determinants of host seeking in soil-transmitted mammalian-parasitic nematodes. Int J Parasitol Drugs Drug Resist. 2018 Dec;8(3):496–510.

21. Fraser LM, Madriz I, Srinivasan D, Zamanian M, Bartholomay L, Kimber M. Chemosensory structure and function in the filarial nematode, Brugia malayi [Internet]. bioRxiv. 2018 [cited 2018 Nov 5]. p. 427229. Available from: https://www.biorxiv.org/content/early/2018/09/26/427229.full.pdf+html

22. Gunawardena NK, Fujimaki Y, Aoki Y. Chemotactic response of Brugia pahangi infective larvae to jird serum in vitro. Parasitol Res. 2003 Jul;90(4):337–42.

23. Kusaba T, Fujimaki Y, Vincent AL, Aoki Y. In vitro chemotaxis of Brugia pahangi infective larvae to the sera and hemolymph of mammals and lower animals. Parasitol Int. 2008 Jun;57(2):179–84.

24. Mitsui Y, Miura M, Bome DA, Aoki Y. In vitro chemotactic responses of Brugia pahangi infective larvae to sodium ions. J Helminthol. 2012 Dec;86(4):406–9.

25. Taylor AE. The development of Dirofilaria immitis in the mosquito Aedes aegypti. J Helminthol. 1960;34:27–38.

26. Bargmann CI. Chemosensation in C. elegans. WormBook. 2006 Oct 25;1–29.

27. Komatsu H, Mori I, Rhee J-S, Akaike N, Ohshima Y. Mutations in a Cyclic Nucleotide–Gated Channel Lead to Abnormal Thermosensation and Chemosensation in C. elegans. Neuron. 1996 Oct 1;17(4):707–18.

28. Coburn CM, Bargmann CI. A Putative Cyclic Nucleotide–Gated Channel Is Required for Sensory Development and Function in C. elegans. Neuron. 1996 Oct 1;17(4):695–706.

29. Colbert HA, Smith TL, Bargmann CI. OSM-9, a novel protein with structural similarity to channels, is required for olfaction, mechanosensation, and olfactory adaptation in Caenorhabditis elegans. J Neurosci. 1997 Nov 1;17(21):8259–69.

30. Tobin DM, Madsen DM, Kahn-Kirby A, Peckol EL, Moulder G, Barstead R, et al. Combinatorial expression of TRPV channel proteins defines their sensory functions and subcellular localization in C. elegans neurons. Neuron. 2002 Jul 18;35(2):307–18.

31. Ressler KJ, Sullivan SL, Buck LB. A zonal organization of odorant receptor gene expression in the olfactory epithelium. Cell. 1993 May 7;73(3):597–609.

32. Vassar R, Ngai J, Axel R. Spatial segregation of odorant receptor expression in the mammalian olfactory epithelium. Cell. 1993 Jul 30;74(2):309–18.

33. Vidal B, Aghayeva U, Sun H, Wang C, Glenwinkel L, Bayer EA, et al. An atlas of Caenorhabditis elegans chemoreceptor expression. PLoS Biol. 2018 Jan;16(1):e2004218.

34. International Helminth Genomes Consortium. Comparative genomics of the major parasitic worms. Nat Genet [Internet]. 2018 Nov 5; Available from: http://dx.doi.org/10.1038/s41588-018-0262-1
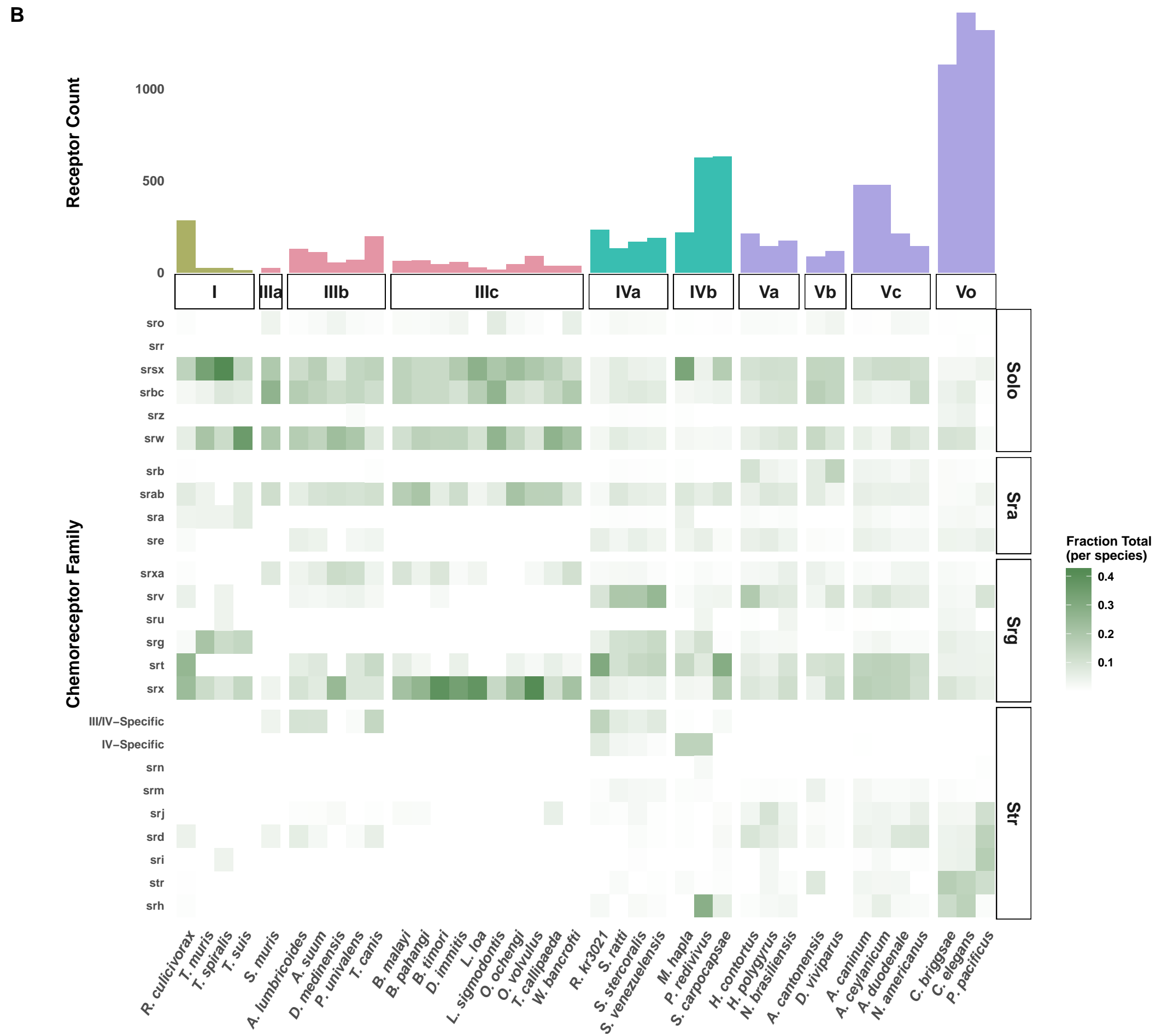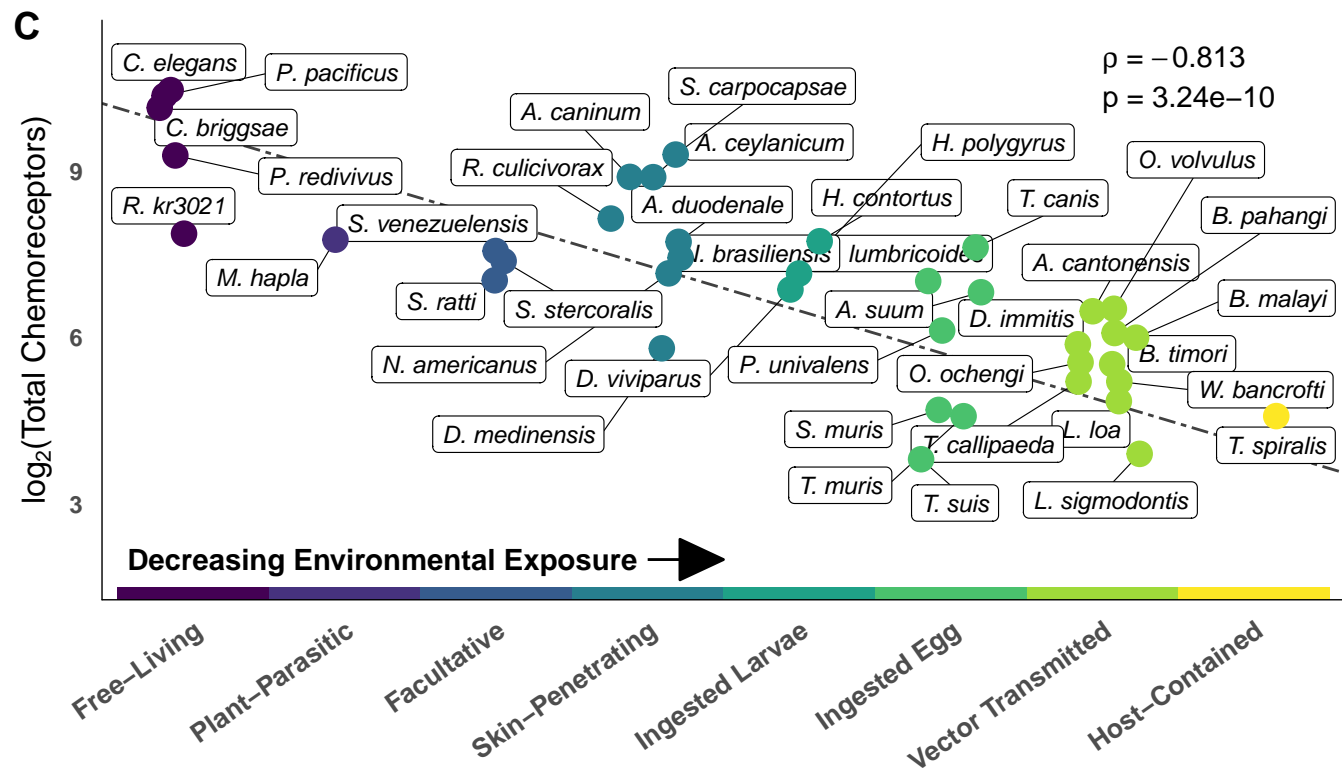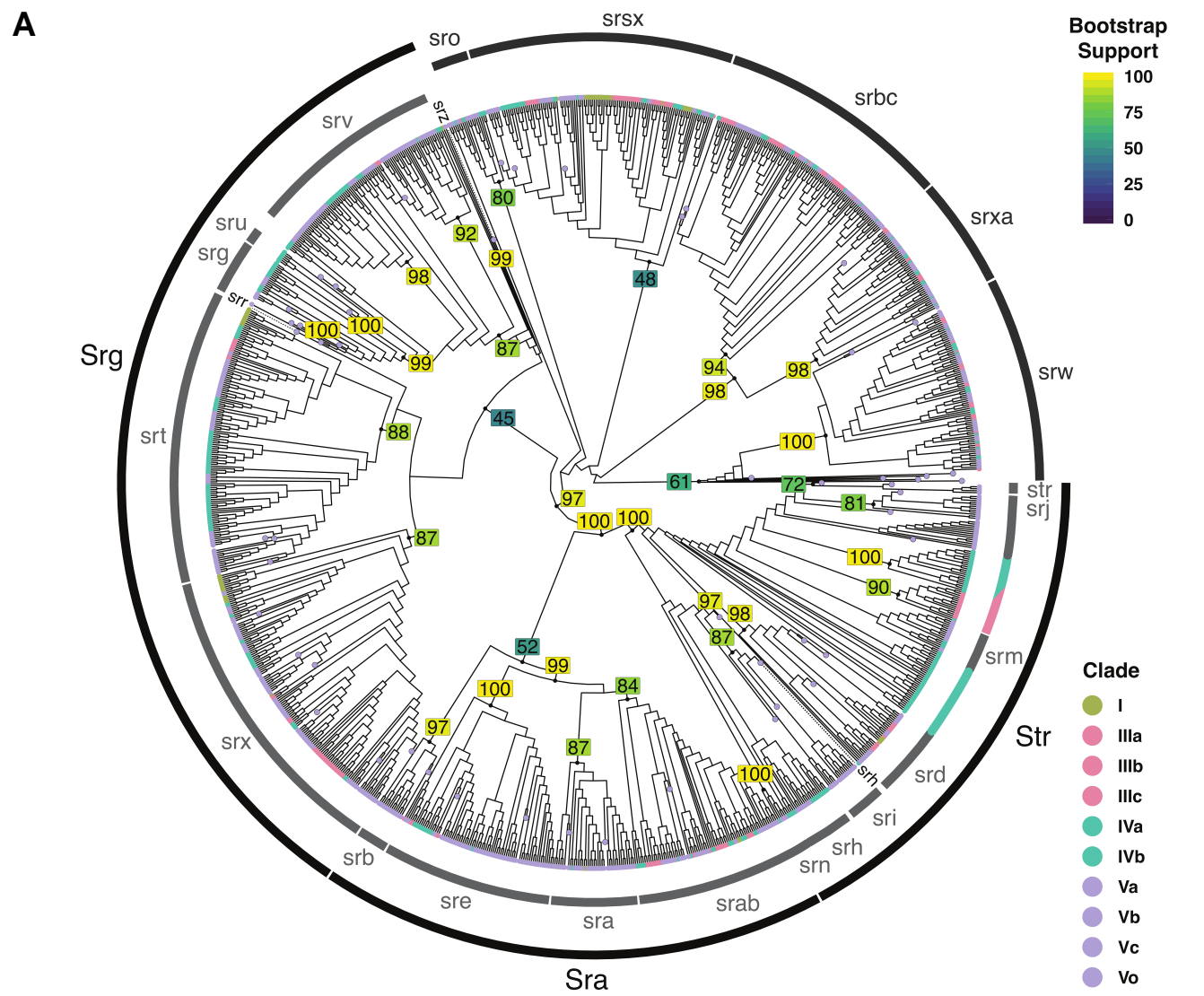
35. Howe KL, Bolt BJ, Shafie M, Kersey P, Berriman M. WormBase ParaSite - a comprehensive resource for helminth genomics. Mol Biochem Parasitol. 2017 Jul;215:2–10.

36. Blaxter M, Koutsovoulos G. The evolution of parasitism in Nematoda. Parasitology. 2015 Feb;142 Suppl 1:S26–39.

37. Thomas JH, Robertson HM. The Caenorhabditis chemoreceptor gene families. BMC Biol. 2008 Oct 6;6:42.

38. Robertson HM, Thomas JH. The putative chemoreceptor families of C. elegans. In: The C. elegans Research Community, editor. WormBook. 2006.

39. Krishnan A, Almén MS, Fredriksson R, Schiöth HB. Insights into the origin of nematode chemosensory GPCRs: putative orthologs of the Srw family are found across several phyla of protostomes. PLoS One. 2014 Mar 24;9(3):e93048.

40. Cotton JA, Bennuru S, Grote A, Harsha B, Tracey A, Beech R, et al. The genome of Onchocerca volvulus, agent of river blindness. Nat Microbiol. 2016 Nov 21;2:16216.

41. Desjardins CA, Cerqueira GC, Goldberg JM, Dunning Hotopp JC, Haas BJ, Zucker J, et al. Genomics of Loa loa, a Wolbachia-free filarial parasite of humans. Nat Genet. 2013 May;45(5):495–500.

42. Jackson AP. Preface. The evolution of parasite genomes and the origins of parasitism. Parasitology. 2015 Feb;142 Suppl 1:S1–5.

43. McLaren DJ. Ultrastructural and cytochemical studies on the sensory organelles and nervous system of Dipetalonema viteae (Nematoda: Filarioidea). Parasitology. 1972 Dec;65(3):507–24.

44. Mclaren DJ. Nematode Sense Organs. In: Dawes B, editor. Advances in Parasitology. Academic Press; 1976. p. 195–265.

45. Liu Z, Kariya MJ, Chute CD, Pribadi AK, Leinwand SG, Tong A, et al. Predator-secreted sulfolipids induce defensive responses in C. elegans. Nat Commun. 2018 Mar 19;9(1):1128.

46. Tran A, Tang A, O'Loughlin CT, Balistreri A, Chang E, Coto Villa D, et al. C. elegans avoids toxin-producing Streptomyces using a seven transmembrane domain chemosensory receptor. Elife [Internet]. 2017 Sep 5;6. Available from: http://dx.doi.org/10.7554/eLife.23770

47. Shtonda BB, Avery L. Dietary choice behavior in Caenorhabditis elegans. J Exp Biol. 2006 Jan;209(Pt 1):89–102.

48. Barrios A, Nurrish S, Emmons SW. Sensory regulation of C. elegans male mate-searching behavior. Curr Biol. 2008 Dec 9;18(23):1865–71.

49. Chung M, Teigen L, Libro S, Bromley RE, Kumar N, Sadzewicz L, et al. Multispecies Transcriptomics Data Set of Brugia malayi, Its Wolbachia Endosymbiont wBm, and Aedes aegypti across the B. malayi Life Cycle. Microbiol Resour Announc [Internet]. 2018 Nov;7(18). Available from: http://dx.doi.org/10.1128/MRA.01306-18

50. Blaxter ML, De Ley P, Garey JR, Liu LX, Scheldeman P, Vierstraete A, et al. A molecular evolutionary framework for the phylum Nematoda. Nature. 1998 Mar 5;392:71.

51. Kindt KS, Viswanath V, Macpherson L, Quast K, Hu H, Patapoutian A, et al. Caenorhabditis elegans TRPA-1 functions in mechanosensation. Nat Neurosci. 2007 May;10(5):568–77.

52. Xing J, Yan X, Estevez A, Strange K. Highly Ca2+-selective TRPM channels regulate IP3-dependent

oscillatory Ca2+ signaling in the C. elegans intestine. J Gen Physiol. 2008 Mar;131(3):245–55.

53. Smith HK, Luo L, O'Halloran D, Guo D, Huang X-Y, Samuel ADT, et al. Defining specificity determinants of cGMP mediated gustatory sensory transduction in Caenorhabditis elegans. Genetics. 2013 Aug;194(4):885–901.

54. Upadhyay A, Pisupati A, Jegla T, Crook M, Mickolajczyk KJ, Shorey M, et al. Nicotinamide is an endogenous agonist for a C. elegans TRPV OSM-9 and OCR-4 channel. Nat Commun. 2016 Oct 12;7:13135.

55. Frim J, Livingstone SD, Reed LD, Nolan RW, Limmer RE. Body composition and skin temperature variation. J Appl Physiol. 1990 Feb;68(2):540–3.

56. Vrablik TL, Huang L, Lange SE, Hanna-Rose W. Nicotinamidase modulation of NAD+ biosynthesis and nicotinamide levels separately affect reproductive development and cell survival in C. elegans. Development. 2009 Nov;136(21):3637–46.

57. Wang W, McReynolds MR, Goncalves JF, Shu M, Dhondt I, Braeckman BP, et al. Comparative Metabolomic Profiling Reveals That Dysregulated Glycolysis Stemming from Lack of Salvage NAD+ Biosynthesis Impairs Reproductive Development in Caenorhabditis elegans. J Biol Chem. 2015 Oct 23;290(43):26163–79.

58. Hashimoto T, Horikawa M, Nomura T, Sakamoto K. Nicotinamide adenine dinucleotide extends the lifespan of Caenorhabditis elegans mediated by sir-2.1 and daf-16. Biogerontology. 2010 Feb;11(1):31–43.

59. Schmeisser K, Parker JA. Nicotinamide-N-methyltransferase controls behavior, neurodegeneration and lifespan by regulating neuronal autophagy. PLoS Genet. 2018 Sep 7;14(9):e1007561.

60. Schmeisser K, Mansfeld J, Kuhlow D, Weimer S, Priebe S, Heiland I, et al. Role of sirtuins in lifespan regulation is linked to methylation of nicotinamide. Nat Chem Biol. 2013 Nov;9(11):693–700.

61. Song C, Gallup JM, Day TA, Bartholomay LC, Kimber MJ. Development of an in vivo RNAi protocol to investigate gene function in the filarial nematode, Brugia malayi. PLoS Pathog. 2010 Dec 23;6(12):e1001239.

62. Grant WN. Transformation of Caenorhabditis elegans with genes from parasitic nematodes. Parasitol Today. 1992 Oct;8(10):344–6.

63. Kwa MS, Veenstra JG, Van Dijk M, Roos MH. Beta-tubulin genes from the parasitic nematode Haemonchus contortus modulate drug resistance in Caenorhabditis elegans. J Mol Biol. 1995 Mar 3;246(4):500–10.

64. Biirglin TR, Lobosb E, Blaxterc ML. Caenorhabditis elegans as a model for parasitic nematodes. Int J Parasitol. 1998;28:395–411.

65. Gillan V, Maitland K, McCormack G, Him NAIIN, Devaney E. Functional genomics of hsp-90 in parasitic and free-living nematodes. Int J Parasitol. 2009 Aug;39(10):1071–81.

66. Law W, Wuescher LM, Ortega A, Hapiak VM, Komuniecki PR, Komuniecki R. Heterologous Expression in Remodeled C. elegans: A Platform for Monoaminergic Agonist Identification and Anthelmintic Screening. PLoS Pathog. 2015 Apr;11(4):e1004794.

67. Wojtyniak M, Brear AG, O'Halloran DM, Sengupta P. Cell- and subunit-specific mechanisms of CNG channel ciliary trafficking and localization in C. elegans. J Cell Sci. 2013 Oct 1;126(Pt 19):4381–95.

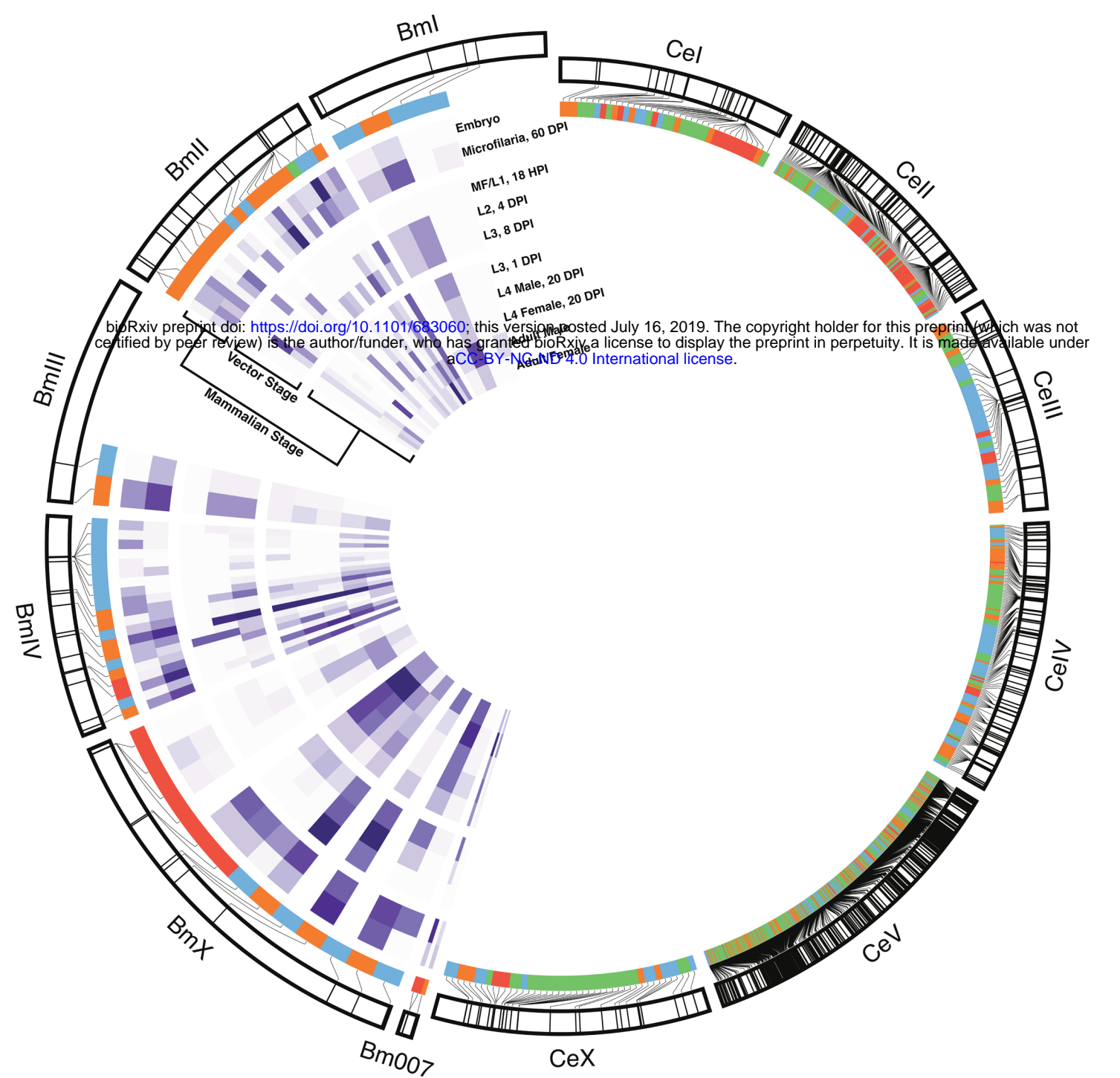68. Komatsu H, Jin YH, L'Etoile N, Mori I, Bargmann CI, Akaike N, et al. Functional reconstitution of a

heteromeric cyclic nucleotide-gated channel of Caenorhabditis elegans in cultured cells. Brain Res. 1999 Mar 6;821(1):160–8.

69. Sengupta P, Chou JH, Bargmann CI. odr-10 encodes a seven transmembrane domain olfactory receptor required for responses to the odorant diacetyl. Cell. 1996 Mar 22;84(6):899–909.

70. Kim K, Sato K, Shibuya M, Zeiger DM, Butcher RA, Ragains JR, et al. Two chemoreceptors mediate developmental effects of dauer pheromone in C. elegans. Science. 2009 Nov 13;326(5955):994–8.

71. Taniguchi G, Uozumi T, Kiriyama K, Kamizaki T, Hirotsu T. Screening of odor-receptor pairs in Caenorhabditis elegans reveals different receptors for high and low odor concentrations. Sci Signal. 2014 Apr 29;7(323):ra39.

72. McGrath PT, Xu Y, Ailion M, Garrison JL, Butcher RA, Bargmann CI. Parallel evolution of domesticated Caenorhabditis species targets pheromone receptor genes. Nature. 2011 Aug 17;477(7364):321–5.

73. Dennis EJ, Dobosiewicz M, Jin X, Duvall LB, Hartman PS, Bargmann CI, et al. A natural variant and engineered mutation in a GPCR promote DEET resistance in C. elegans. Nature. 2018 Oct;562(7725):119–23.

74. Zhang C, Zhao N, Chen Y, Zhang D, Yan J, Zou W, et al. The Signaling Pathway of Caenorhabditis elegans Mediates Chemotaxis Response to the Attractant 2-Heptanone in a Trojan Horse-like Pathogenesis. J Biol Chem. 2016 Nov 4;291(45):23618–27.

75. Park D, O'Doherty I, Somvanshi RK, Bethke A, Schroeder FC, Kumar U, et al. Interaction of structure-specific and promiscuous G-protein–coupled receptors mediates small-molecule signaling in Caenorhabditis elegans. Proc Natl Acad Sci U S A. 2012 Jun 19;109(25):9917–22.

76. Greene JS, Dobosiewicz M, Butcher RA, McGrath PT, Bargmann CI. Regulatory changes in two chemoreceptor genes contribute to a Caenorhabditis elegans QTL for foraging behavior. Elife [Internet]. 2016 Nov 28;5. Available from: http://dx.doi.org/10.7554/eLife.21454

77. Wan X, Zhou Y, Chan CM, Yang H, Yeung C, Chow KL. SRD-1 in AWA neurons is the receptor for female volatile sex pheromones in C. elegans males. EMBO Rep [Internet]. 2019 Mar;20(3). Available from: http://dx.doi.org/10.15252/embr.201846288

78. Liu C, Mhashilkar AS, Chabanon J, Xu S, Lustigman S, Adams JH, et al. Development of a toolkit for piggyBac-mediated integrative transfection of the human filarial parasite Brugia malayi. PLoS Negl Trop Dis. 2018 May;12(5):e0006509.

79. Gray JM, Karow DS, Lu H, Chang AJ, Chang JS, Ellis RE, et al. Oxygen sensation and social feeding mediated by a C. elegans guanylate cyclase homologue. Nature. 2004 Jul 15;430(6997):317–22.

80. Glauser DA, Chen WC, Agin R, Macinnis BL, Hellman AB, Garrity PA, et al. Heat avoidance is regulated by transient receptor potential (TRP) channels and a neuropeptide signaling pathway in Caenorhabditis elegans. Genetics. 2011 May;188(1):91–103.

81. Hilliard MA, Apicella AJ, Kerr R, Suzuki H, Bazzicalupo P, Schafer WR. In vivo imaging of C. elegans ASH neurons: cellular response and adaptation to chemical repellents. EMBO J. 2005 Jan 12;24(1):63–72.

82. He C, Altshuler-Keylin S, Daniel D, L'Etoile ND, O'Halloran D. The cyclic nucleotide gated channel subunit CNG-1 instructs behavioral outputs in Caenorhabditis elegans by coincidence detection of

nutritional status and olfactory input. Neurosci Lett. 2016 Oct 6;632:71–8.

83. O'Halloran DM, Altshuler-Keylin S, Zhang X-D, He C, Morales-Phan C, Yu Y, et al. Contribution of the cyclic nucleotide gated channel subunit, CNG-3, to olfactory plasticity in Caenorhabditis elegans. Sci Rep. 2017 Mar 13;7(1):169.

84. Haas W. Parasitic worms: strategies of host finding, recognition and invasion. Zoology . 2003;106(4):349–64.

85. Rutledge LC, Ward RA, Gould DJ. Studies on the feeding response of mosquitoes to nutritive solutions in a new membrane feeder. Mosquito News. 1964;24(4):407–19.

86. Hayes RO. Determination of a Physiological Saline Solution for Aedes aegypti (L.). J Econ Entomol. 1953 Aug 1;46(4):624–7.

87. Mello C, Fire A. Chapter 19 DNA Transformation. In: Epstein HF, Shakes DC, editors. Methods in Cell Biology. Academic Press; 1995. p. 451–82.

88. Mistry J, Finn RD, Eddy SR, Bateman A, Punta M. Challenges in homology search: HMMER3 and convergent evolution of coiled-coil regions. Nucleic Acids Res. 2013 Jul;41(12):e121.

89. Punta M, Coggill PC, Eberhardt RY, Mistry J, Tate J, Boursnell C, et al. The Pfam protein families database. Nucleic Acids Res. 2012 Jan;40(Database issue):D290–301.

90. Camacho C, Coulouris G, Avagyan V, Ma N, Papadopoulos J, Bealer K, et al. BLAST+: architecture and applications. BMC Bioinformatics. 2009 Dec 15;10:421.

91. Harris TW, Antoshechkin I, Bieri T, Blasiar D, Chan J, Chen WJ, et al. WormBase: a comprehensive resource for nematode research. Nucleic Acids Res. 2010 Jan;38(Database issue):D463–7.

92. Katoh K, Standley DM. MAFFT multiple sequence alignment software version 7: improvements in performance and usability. Mol Biol Evol. 2013 Apr;30(4):772–80.

93. Edgar RC. MUSCLE: multiple sequence alignment with high accuracy and high throughput. Nucleic Acids Res. 2004 Mar 19;32(5):1792–7.

94. Tusnády GE, Simon I. The HMMTOP transmembrane topology prediction server. Bioinformatics. 2001 Sep;17(9):849–50.

95. Capella-Gutiérrez S, Silla-Martínez JM, Gabaldón T. trimAl: a tool for automated alignment trimming in large-scale phylogenetic analyses. Bioinformatics. 2009 Aug 1;25(15):1972–3.

96. Nguyen L-T, Schmidt HA, von Haeseler A, Minh BQ. IQ-TREE: a fast and effective stochastic algorithm for estimating maximum-likelihood phylogenies. Mol Biol Evol. 2014;32(1):268–74.

97. Kalyaanamoorthy S, Minh BQ, Wong TKF, von Haeseler A, Jermiin LS. ModelFinder: fast model selection for accurate phylogenetic estimates. Nat Methods. 2017 Jun;14(6):587–9.

98. Hoang DT, Chernomor O, von Haeseler A, Minh BQ, Vinh LS. UFBoot2: Improving the Ultrafast Bootstrap Approximation. Mol Biol Evol. 2018 Feb 1;35(2):518–22.

99. Müller T, Vingron M. Modeling amino acid replacement. J Comput Biol. 2000;7(6):761–76.

100. Yang Z. A space-time process model for the evolution of DNA sequences. Genetics. 1995 Feb;139(2):993–1005.

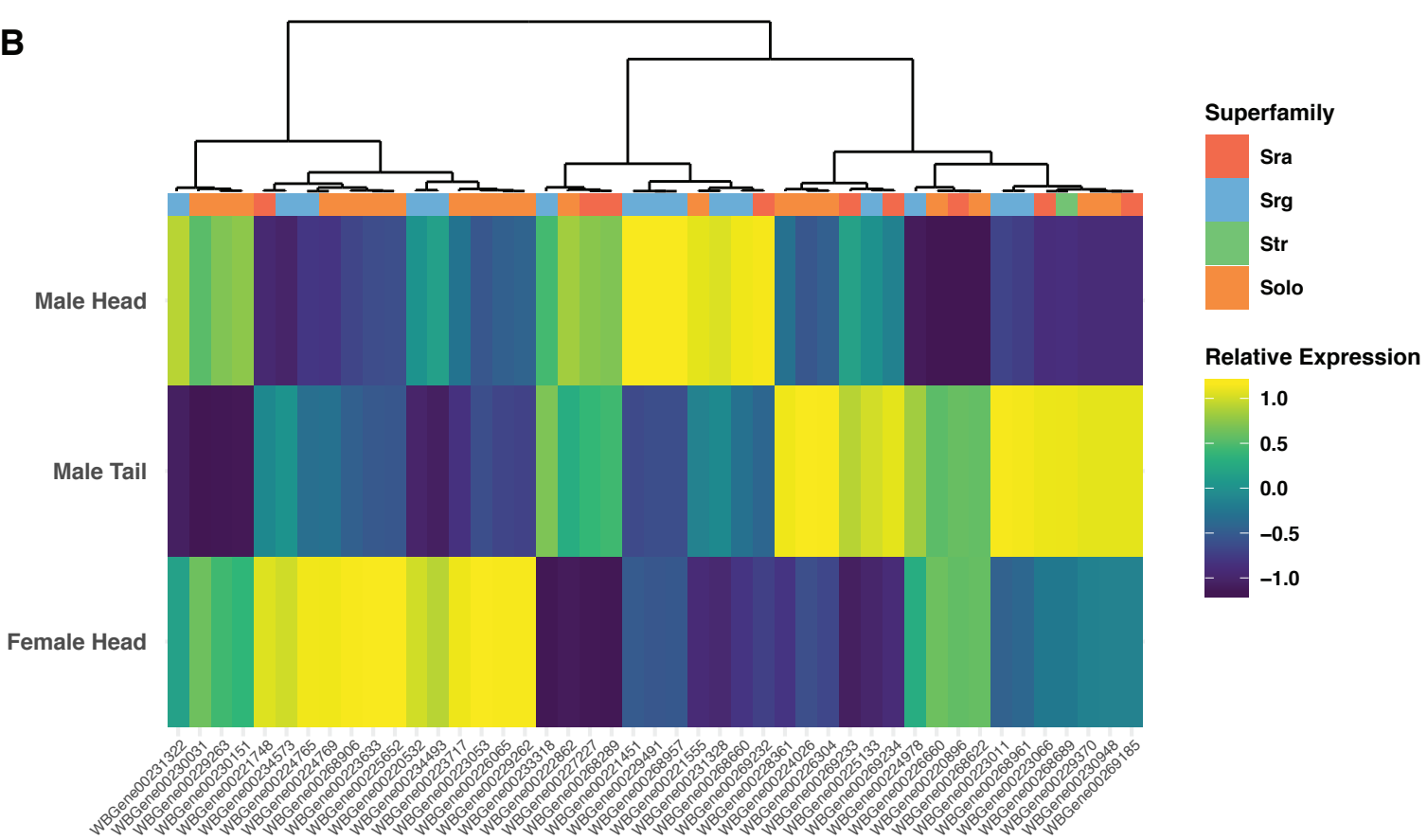101. Soubrier J, Steel M, Lee MSY, Der Sarkissian C, Guindon S, Ho SYW, et al. The influence of rate

heterogeneity among sites on the time dependence of molecular rates. Mol Biol Evol. 2012 Nov;29(11):3345–58.

102.   Ronquist F, Teslenko M, van der Mark P, Ayres DL, Darling A, Höhna S, et al. MrBayes 3.2: efficient Bayesian phylogenetic inference and model choice across a large model space. Syst Biol. 2012 May;61(3):539–42.

103.   Yu G, Smith DK, Zhu H, Guan Y, Lam TT-Y. ggtree : an r package for visualization and annotation of phylogenetic trees with their covariates and other associated data. McInerny G, editor. Methods Ecol Evol. 2017 Jan 22;8(1):28–36.

104.   Bolger AM, Lohse M, Usadel B. Trimmomatic: a flexible trimmer for Illumina sequence data. Bioinformatics. 2014 Aug 1;30(15):2114–20.

105.   Kim D, Langmead B, Salzberg SL. HISAT: a fast spliced aligner with low memory requirements. Nat Methods. 2015 Apr;12(4):357–60.

106.   Pertea M, Pertea GM, Antonescu CM, Chang T-C, Mendell JT, Salzberg SL. StringTie enables improved reconstruction of a transcriptome from RNA-seq reads. Nat Biotechnol. 2015 Mar;33(3):290–5.

107.   Di Tommaso P, Chatzou M, Floden EW, Barja PP, Palumbo E, Notredame C. Nextflow enables reproducible computational workflows. Nat Biotechnol. 2017 Apr 11;35(4):316–9.

108.   Krzywinski M, Schein J, Birol I, Connors J, Gascoyne R, Horsman D, et al. Circos: an information aesthetic for comparative genomics. Genome Res. 2009 Sep;19(9):1639–45.

109.   Wickham H, Grolemund G. R for Data Science: Import, Tidy, Transform, Visualize, and Model Data. "O'Reilly Media, Inc."; 2016. 492 p.

110.   Schindelin J, Arganda-Carreras I, Frise E, Kaynig V, Longair M, Pietzsch T, et al. Fiji: an open-source platform for biological-image analysis. Nat Methods. 2012 Jun 28;9(7):676–82.

111.   Ballesteros C, Tritten L, O'Neill M, Burkman E, Zaky WI, Xia J, et al. The Effect of In Vitro Cultivation on the Transcriptome of Adult Brugia malayi. PLoS Negl Trop Dis. 2016 Jan;10(1):e0004311.

112.   Untergasser A, Cutcutache I, Koressaar T, Ye J, Faircloth BC, Remm M, et al. Primer3--new capabilities and interfaces. Nucleic Acids Res. 2012 Aug;40(15):e115.

113.   Schmittgen TD, Livak KJ. Analyzing real-time PCR data by the comparative C(T) method. Nat Protoc. 2008;3(6):1101–8.

114.   Thorvaldsdóttir H, Robinson JT, Mesirov JP. Integrative Genomics Viewer (IGV): high-performance genomics data visualization and exploration. Brief Bioinform. 2013 Mar;14(2):178–92.

115.   Altschul SF, Gish W, Miller W, Myers EW, Lipman DJ. Basic local alignment search tool. J Mol Biol. 1990 Oct 5;215(3):403–10.

116.   Bargmann CI, Hartwieg E, Horvitz HR. Odorant-selective genes and neurons mediate olfaction in C. elegans. Cell. 1993 Aug 13;74(3):515–27.
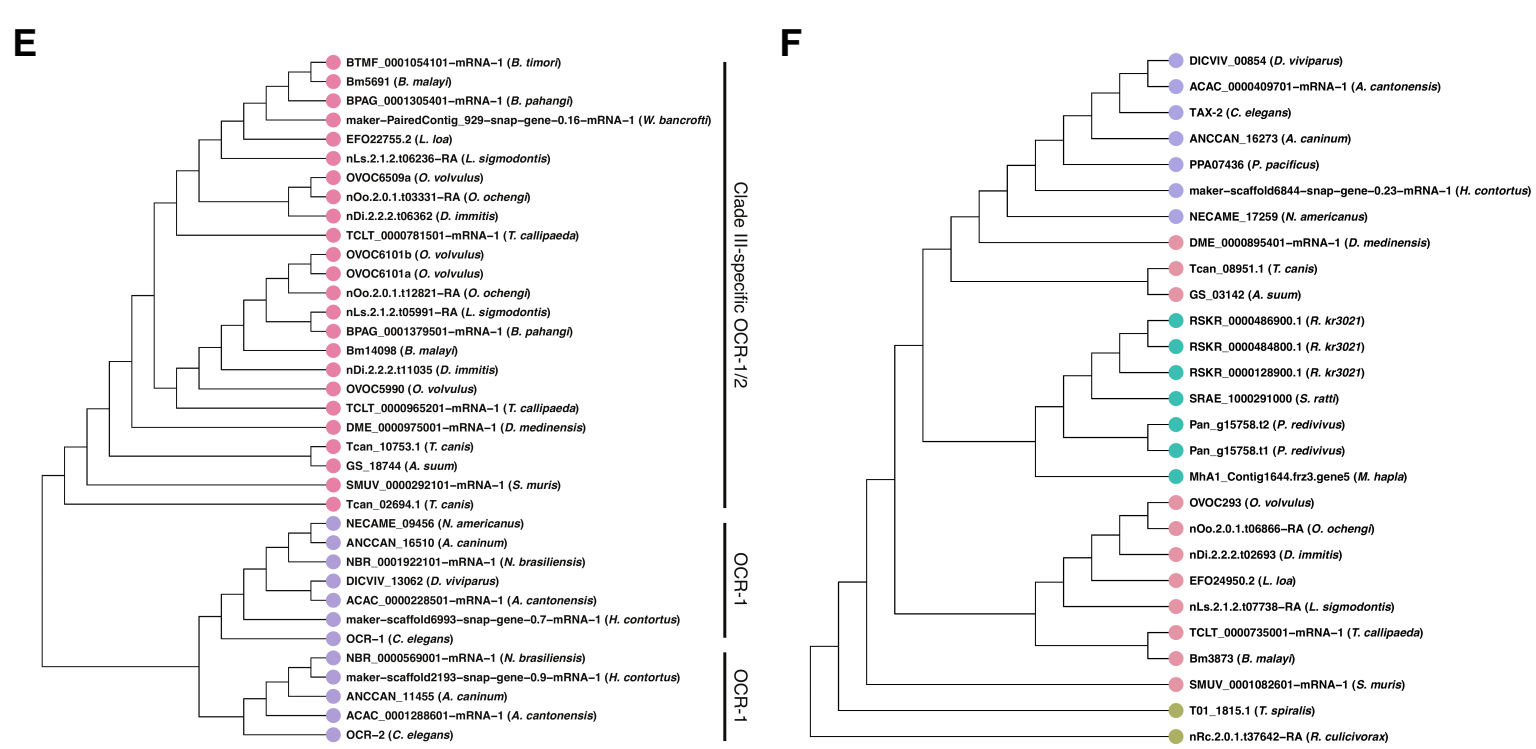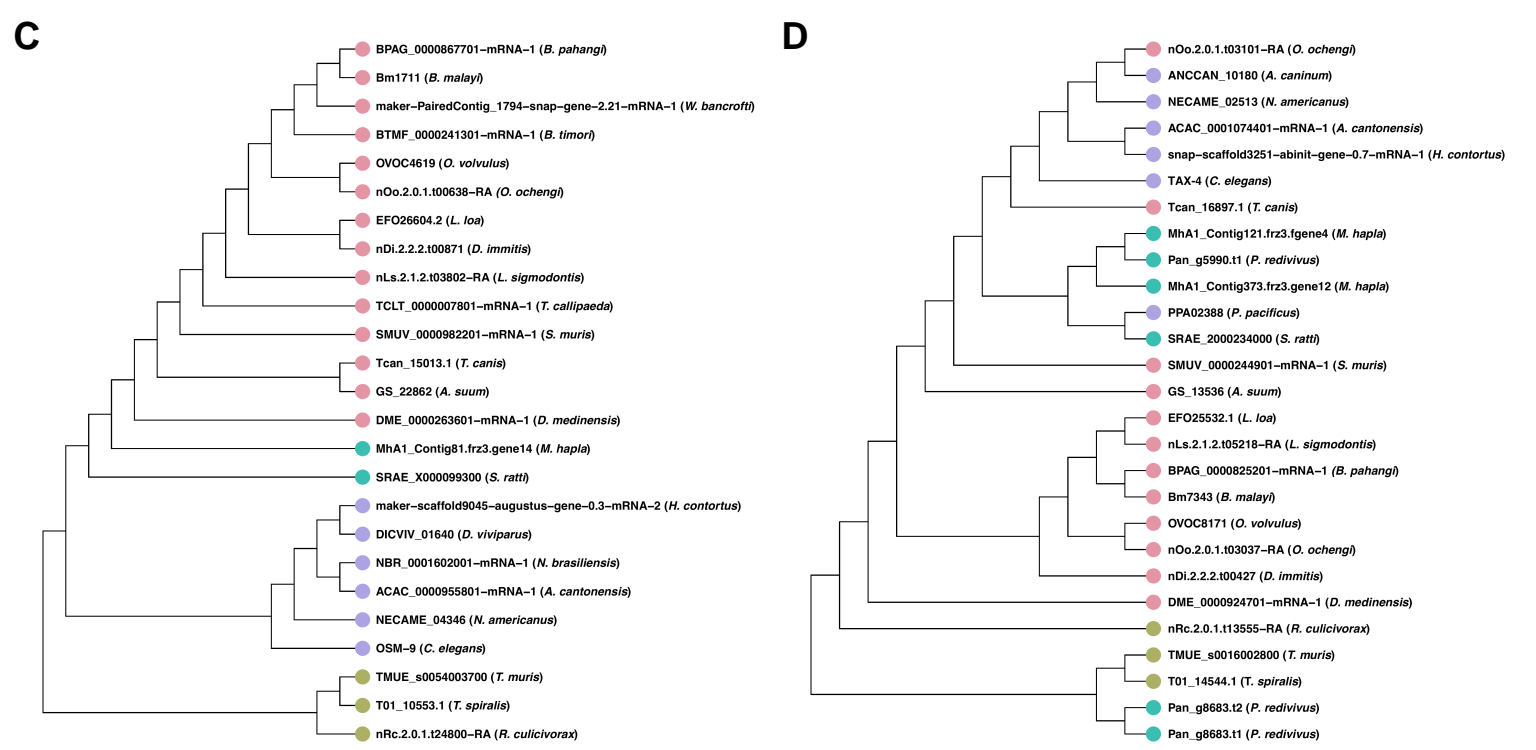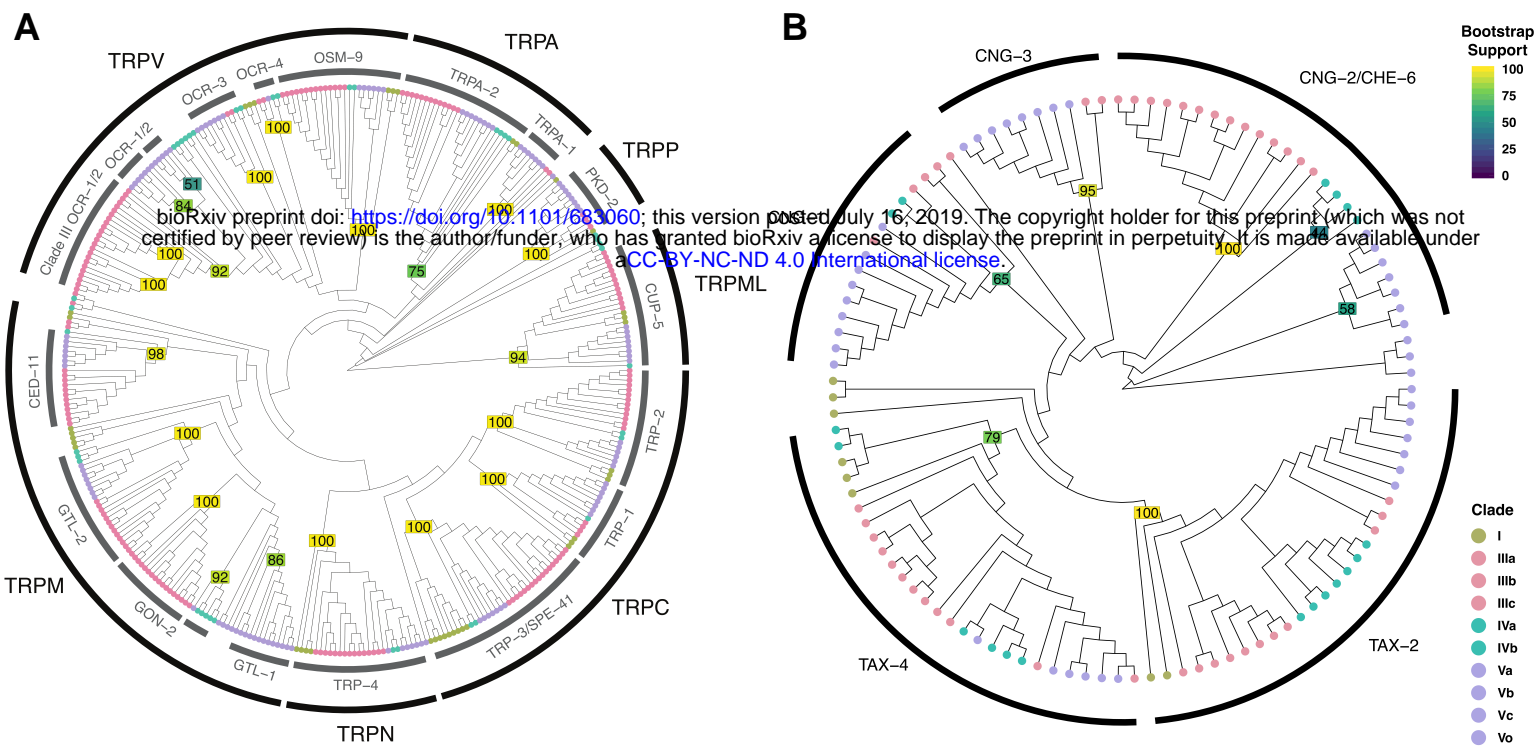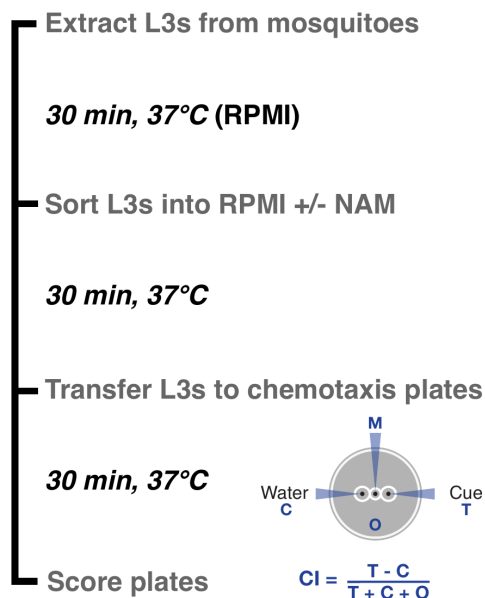
A

BmI · CeI · CeII · CeIII · CeIV · BmII · BmIII · BmIV · BmX · Bm007 · CeX · CeV

Embryo
Microfilaria, 60 DPI
MF/L1, 18 HPI
L2, 4 DPI
L3, 8 DPI
L3, 1 DPI
L4 Male, 20 DPI
L4 Female, 20 DPI
Adult Male
Adult Female

Vector Stage
Mammalian Stage

B

Superfamily
- Sra
- Srg
- Str
- Solo

Relative Expression
1.0
0.5
0.0
-0.5
-1.0

Male Head · Male Tail · Female Head

A Extract L3s from mosquitoes

30 min, 37°C (RPMI)

Sort L3s into RPMI +/- NAM

30 min, 37°C

Transfer L3s to chemotaxis plates

30 min, 37°C

Score plates

$$CI = \frac{T - C}{T + C + O}$$

B 0 DPE

FBS — Mean CI: 0.91 — **

NaCl — Mean CI: 0.69 — **

3–methyl–1–butanol — Mean CI: –0.46 — ns

Chemotaxis Index (CI)

Untreated / NAM

C 0 DPE — ns

Fraction leaving center

Untreated / NAM

D $\Delta\Delta C_T$

4 HPE, 37°C vs. 0 HPE

4 HPE, 21°C vs. 0 HPE

E 1 DPE — FBS — Mean CI: 0

Chemotaxis Indexi (CI)

Untreated

1 DPE

Fraction leaving center

Untreated

A

Add L3s to NAM plate

24 hr, 37°C

Temperature switch

20 min, 21°C

Record 📷

10 sec, 21°C

Repeat cooling and recording after 48 hr

B

Control

1 mM NAM

C

24hr

48hr

A

0 DPI

MF · L1 · L2 · L3

Thoracic musculature · Head / Proboscis

Hemocoel

Midgut

~10 L3s

M

Water · Serum

C · T

O

B

Chemotaxis Index (CI)

***

****

lacZ(RNAi) · osm-9(RNAi) · tax-4(RNAi)

Fraction Leaving Center

ns

ns

lacZ(RNAi) · osm-9(RNAi) · tax-4(RNAi)

A Diacetyl

B Isoamyl alcohol

Chemotaxis Index

N2   osm-9(ky10)   osm-9(ky10); osm-9p::bm-osm-9

N2   tax-4(p678)   tax-4(p678); tax-4p::bm-tax-4

**** ns **** ns **** ****